
Signal Theory and Communications Department

# Smart Beamforming for 5G and LTE Legacy Systems

Carles Díaz Vilor

---

Supervised by:
Ana Isabel Pérez Neira

# Abstract

The new generation of wireless communication systems is expected to provide many features and advances for a variety of use cases. In addition, the basis of 5G, being the Long Term Evolution (LTE) will be developed in parallel, meaning that further improvements need to be done in both technologies. In this work we propose two novel schemes, one for each generation, that provide potential benefits for the scenarios in which we are focused, in terms of Bit Error Rate (BER), Probability of Collision and/or achievable Rate as we will see. Firstly, massive Machine Type Communications (mMTC) is a multi-user and multi-service air interface which will be key in the next generation of communications. In this work, we propose a frame structure and signal processing techniques at the receiver needed to create the beamformers whose final objective is reducing the probability of collision between devices trying to get the resources. In the end, this will imply that more users can access to the media, as the receiver would be able to manage the collisions that will occur in the frequency domain, being the case of a Non-Orthogonal-Multiple-Access. Second, as there is an increasing interest in rapidly varying channels, we focus on this aspect proposing a frame structure for LTE in which we are able to track better the channel in case it has a low coherence time, that in combination with beamforming techniques will help the system to null interferences from other users and to increase the Signal to Interference and Noise Ratio (SINR) yielding to a lower BER. In the same chapter, in addition, we try to figure out which is the best power allocation with respect to the SNR to mix both training and data to even increase more the rate with respect to LTE without degrading the BER so much. We expect this work will be useful for the development of the technologies which are said that will improve our lifestyles.

As soon as the registration for the IEEE International Conference on Communications (IEEE ICC) 2020 opens, we will submit an article regarding the part of this Master Thesis dealing with 5G-mMTC. Its title is: ***RSBA-Resource Sharing Beamforming Access for 5G-mMTC*** and is annexed apart from this document and uploaded to the ETSETB-Intranet.

# Acknowledgments

I want to dedicate this section to the people that has helped me during my Final Master Thesis. Firstly, I would like to thank my advisor Ana Isabel Pérez Neira for the knowledge and help that has provided me throughout this time.

Finally, thanks to my parents for the support that they have given me during this period.

# Contents

# List of Figures

# Chapter 1

# Introduction

Nowadays, we live in a world in which the emergence of new communication systems force both industry and academia to work hard in order to keep evolving the state of the art technologies. The easiest example may be the 5G-NR (New Radio), which is said that will change our lives in many senses. From the user experience to the speed systems are capable to transmit information. Such technology is based on the existing ones, mainly in 4G-LTE with the addition of features that make the objectives of 5G feasible. Despite that, such large evolutions take long times, thus, we will have to wait some years until 5G is completely installed in our lives. In parallel, LTE will be developed too, being key for the new technology, wherewith it is important to remark that we should never forget the great impact LTE has, and will have.

It is widely known that each technology has its own protocol, containing different layers, such as the physical (PHY), multiple access control (MAC) up to the application layers. In this work we will focus on the PHY layer of LTE and 5G communication systems. In particular, different PHY-layer techniques will be developed with the aim of achieving better performances with respect to the state-of-the-art techniques, with the guess that they will be widely used in many applications, such as in Internet of Things (IoT), Satellite Communications or industry procedures.

In particular, the most studied PHY-layer technique in this work is beamforming. Its main objective is to spatially filter the received signal and only allow the ones that have a particular spatial signature, being a Spatial-Division Multiple Access (SDMA). In other words, it filters signals in such a way that only the ones fulfilling a set of features will be seen at the output. The easiest example to understand the idea is the Time-Reference (TR) beamforming, in which we create the combiner in such a way that its output should be similar to a time-domain reference sequence, the so called training sequence. In the end, the beamformer will point to the device that transmits what we expect to receive. Hence, beamforming can be used as a SDMA technique or user discrimination based on the spatial signature. The main benefit of such pointing is the increase in the Signal to Noise Ratio (SNR). Moreover, depending on the problem, apart from pointing to a user of interest, we may be interested in nulling possible interferences, so the beamformer response would also increase the Signal to Interference and Noise Ratio (SINR). Apart from the properties of the involved signals, another important parameter in PHY-layer techniques is the number of antennas. It is important for three main reasons. First, the more antennas we have, the narrower will be the beams. Second, it determines the degrees of freedom we have in the system, and, finally, as we will see during the work, we require to estimate correlation matrixes and vectors, meaning that we need a representative number of samples to make such estimation. The more antennas we have, the more samples we will need to provide reliable estimates.

Another important point that must be taken into account when designing beamformers is the working frequency and its operation bandwidth. Both 4G and 5G work with the Orthogonal Frequency Division Multiplexing (OFDM) technique, meaning that the symbols will be located at different subcarriers, therefore, depending on the beamformer and the bandwidth of the signal it may happen that the frequency domain response of the spatial processor is not flat. These type of combiners are known as Wide-Band, and may present some inconveniences, as they imply the computation

of a beamvector for each subcarrier. The other kind of beamformers are known as Narrow-Band, meaning that the response in the frequency domain is flat, with the advantage that one beamformer could cover the whole bandwidth of the signal, therefore a great amount of computations would be avoided. The condition for a beamformer to be Narrow-Band is the following one: $\frac{D}{\lambda} \ll \frac{f_c}{B}$ where $\lambda$ is the wavelength of the signal, $D$ is the separation between antenna elements, $f_c$ is the carrier frequency and $B$ is the bandwidth of the signal. For the signals and frequencies used in this work, the Narrow-Band contition is fulfilled, so from now till the end of the work we can ensure that the beamformers we present, satisfy a flat frequency response in the band of interest.

As previously stated, we will focus our efforts on 4G-LTE and 5G scenarios. Starting the discussion with the newest technology, being the 5G, there are three main targets. The first one is related to Enhanced Mobile Broadband (eMBB), which would allow higher rates and improve spectral efficiency. The main difference with respect to 4G-LTE in this point are the bandwidths 5G will use (up to 400 MHz vs 20 MHz in LTE). The second objective of 5G is providing Ultra-Reliable and Low Latency Communications (URLLC), trying to achieve a latency in the Radio Access Network (RAN) lower than 1ms. Finally, the last target is dealing with Massive Machine-Type Communications (mMTC), being the one that is most related to this work. These kind of communications are thought to support scenarios with a very high density of users. In particular, the hot topic related to mMTC are the Non-Orthogonal-Multiple-Access (NOMA) procedures. Apart from that, the fact that devices can use whatever subcarrier, imply an increase in the efficiency with respect to Orthogonal-Multiple-Access (OMA) techniques. Moreover, serving multiple users re-using bandwidth, also implies the achievement of higher rates. More details on NOMA will be given in an upcoming section of the work.

These main three points will be deployed in the next years, using different bands of the spectrum. For example, in order to achieve the 20 Gbps at the Downlink (DL) 5G has targeted, there is a need of using higher frequencies, in this case, the millimeter wave (mmW) bands. The main drawback of such bands is the short ranges they could cover due to path losses. For other applications, there may be interest in using the Mid (2.3 to 5 GHz) and Low (600 MHz to 2100 MHz) Bands, therefore we can see that depending on the needs, the deployment is one or other.

If we remember the main objective of LTE, was achieving higher peak rates taking benefit from OFDM, which was not used until that moment in wireless communications. Thanks to its easy implementation and myriad benefits, we can say it has been the most important technology in wireless communications so far. We could list many of its advantages, from the aforementioned higher rates to an easier channel equalization, being all of them the reason why OFDM is in charge of the signal transportation in 4G and 5G, therefore in this work we will suppose all signals are OFDM-modulated.

Once the framework of this project has been established, we proceed to post the main objectives of this Final Master Thesis developed at the Technical University of Catalonia. First, we would like to provide the basics for the reader to understand the main aspects of these two key technologies, being the 4G and 5G. In particular, we will cover aspects related to different PHY-layer techniques for 4G and 5G, such as beamforming or channel estimation. It must be said that the work is focused on the Uplink (UL), but could be extrapolated to the DL too. At this point, we will divide our contributions into two. Regarding 5G, this work develops a study of a possible frame structure in a scenario with massive devices in combination with beamforming techniques, with the objective of providing reliable communications allowing frequency-domain overlapping, that is a NOMA access. The second part is focused on 4G-LTE, where we propose a legacy system aiming to achieve higher rates compared to LTE. This method is based on changing the way training sequences are allocated. As we will see, such structure would provide benefits related to tracking or synchronization, apart from the aforementioned increase in the rate. Moreover, we have investigated how to outperform such scheme by means of what we called Super-Imposed training, in which we look for the optimal power allocation to training and data when sending them at the same time, to maximize the SNR at the receiver. We would like to remark that both techniques are novel in the sense that few work has been done in NOMA for the uplink in 5G, and, even less implementing beamforming techniques, and for 4G-LTE we have not found references studying such methods.

The remainder of the work is organized as follows. In Chapter 2 we present the Fundamentals and the framework needed to understand the rest of the thesis. Chapter 3 shows our proposal to combine NOMA with beamforming for 5G scenarios, including both mathematical developments and simulations. In Chapter 4 we present an LTE legacy system, as it is thought to coexist with the existing 4G technologies and, finally, the last chapter is devoted to post the conclusions we have obtained during this Final Master Thesis.

# Chapter 2

# Fundamentals

## 2.1 OFDM Basics

During the last years, the emergence of new signal processing techniques, such as Multiple-Input Multiple-Output (MIMO) or beamforming has provided many benefits, yielding to higher rates or lower error probabilities. Moreover, multi-carrier modulations outperform other technologies when dealing with frequency-selective wireless channels. In particular, OFDM is the most used multi-carrier modulation system as it is able to erase Inter-Symbol Interference (ISI) and create a set of parallel channels in the frequency domain. In case we are able to use multiple antennas at the transmitter and/or at the receiver, spatial diversity can also be a mean to combine properly the received signal in order to reduce the BER.

Regarding OFDM, being the selected technology as the basis for the physical layer of 4G-LTE and 5G, it allows high peak transmission rates with good spectral efficiencies and a scheduling that is able to work with multiple channel bandwidths. In our case, the wireless environment, thanks to the structure that OFDM symbols have, apart from the aforementioned benefits, the use of a Cyclic Prefix (CP) increases robustness against multipath and also limits ISI. This, combined with its simple implementation and/or precoding/decoding strategies make OFDM a key technology in our communication systems.

So let's see how these signals are. Previously, we mentioned that these kind of signals are easy to obtain. That is why we only need one step: the Inverse Fourier Transform (IFFT) operation. In particular, a $N$-point IFFT, being $N$ the total number of subcarriers that are assigned for such bandwidth. Supposing we have a number of symbols, $M$, according to a certain modulation e.g. 4-QAM, 16-QAM denoted by $\mathcal{S} = \{s(1)\,,\, s(2)\,,\, ...\,,\, s(M)\}$, we will map the symbols into $M$ subcarriers of interest. Note that $M \leq N$. Once such mapping has been done, we assign a value of zero to the unused subcarriers, so that a new set is obtained, $\mathcal{S}'$, $|\mathcal{S}'| = N$. Then, the $IFFT\{\mathcal{S}'\}$, where $\mathcal{S}' = \{s'(1)\,,\, s'(2)\,,\, ...\,,\, s'(N)\}$, gives a temporal representation of the symbols mapped in the frequency domain. Finally, in order to obtain the OFDM signal, the CP must be added, being in charge of erasing ISI. At the demodulator, the inverse process would be done in order to recover the initial complex symbols. Figure 2.1 tries to briefly summarize the complete scheme of modulating and demodulating an OFDM signal.

Given the set of mapped symbols $\mathcal{S}' = \{s'(1)\,,\, s'(2)\,,\, ...\,,\, s'(N)\}$, the time domain signal will be given by the following expression:

$$x(n) \;=\; \frac{1}{N} \sum_{i=0}^{N-1} s'(i)\, e^{j2\pi \frac{in}{N}} \tag{2.1}$$

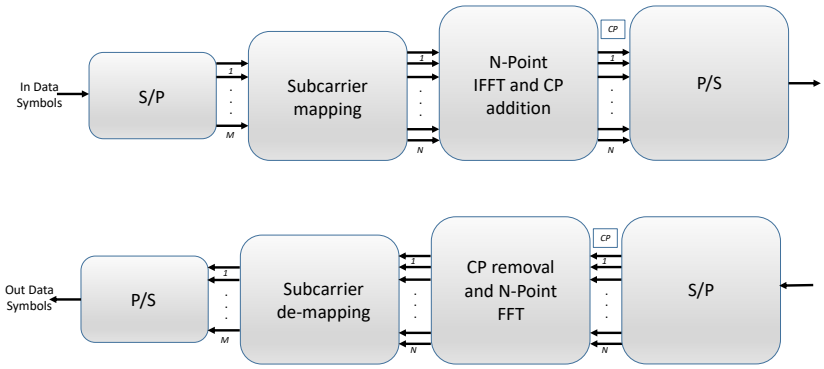


Figure 2.1: Modulation and Demodulation process of the symbols using OFDM technique.

## 2.2 LTE

This second part of the chapter is devoted to explain the fundamentals of the 4G LTE PHY layer. First, we will introduce why is it used the multi-carrier solution, and secondly, as the framework of this Thesis is in the UL, we will enter more into detail about the main characteristics of such link.

### 2.2.1 Basics

Despite the easiness to obtain such signals, the design of the LTE PHY layer has been subject of study for many years, as it has many requirements such as high peak rates, spectral efficiency and many others. It has been mentioned before that the technology who made possible to fulfill them was OFDM. Apart from that, the implementation of other signal processing techniques such as beamforming or MIMO provided even better performances. The combination of these elements among others constitute the major differentiation with respect to previous technologies such as 2G and 3G.

Along the first section we presented OFDM as a key technology that is able to achieve the aforementioned requirements. In particular, as the general scenario will have many devices there is a fundamental aspect that should be taken into account: the multiple access (MA). In LTE, it is done by means of the well-known Orthogonal-Frequency Division Multiple Access (OFDMA), enabling to provide orthogonality among users thanks to specific patterns in time and frequency. Although the DL of the PHY layer is based on OFDMA, it has an important drawback that makes it unfeasible for the UL: the peak-to-average power ratio (PAPR). Instead, Single Carrier Frequency Division Multiple Access (SC-FDMA) is the technology for the UL as it reduces the PAPR and consequently the expensiveness of the UE. It is implemented using a Discrete Fourier Transfrom Spread OFDM (DFTS-OFDM) transmission in which the bandwidth for both UL and DL is determined by the required data rate. See Figure 2.2 to have an idea on how the spectrum of these two techniques look like.

Regarding the time-domain representation of LTE signals, there are different parameters that will help us to understand how they are divided. A complete radio frame lasts 10 ms, containing ten equally sized subframes of 1 ms. Each subframe is divided into two slots of 0.5 ms length, and, finally, inside each slot we can find a number of OFDM/SC-FDMA symbols, in general seven (for normal CP length) or six (in case of extended CP). Regarding the CP, it must be said that its length should be longer than the typical delay spread to fully erase ISI.

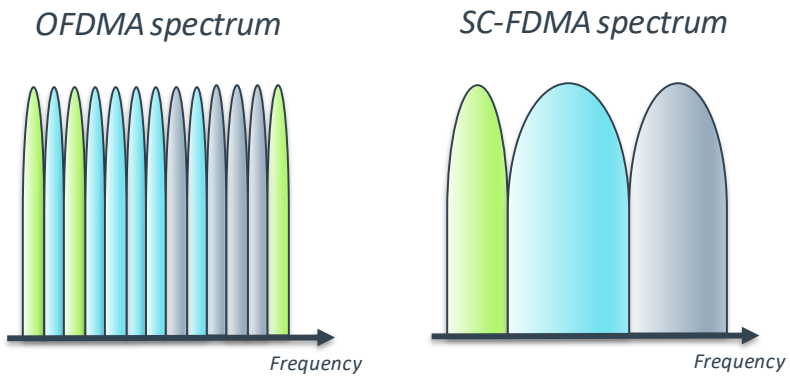


Figure 2.2: OFDMA and SC-FDMA multiuser spectrums.

| Channel Bandwidth (MHz) | 1.4 | 3 | 5 | 10 | 15 | 20 |
|---|---|---|---|---|---|---|
| Frame Duration (ms) | 10 | | | | | |
| Subframe Duration (ms) | 1 | | | | | |
| Subcarrier Spacing (KHz) | 15 | | | | | |
| IFFT Size, $N$ | 128 | 256 | 512 | 1024 | 1536 | 2048 |
| Number of occupied subcarriers (DC included) | 76 | 181 | 301 | 601 | 901 | 1201 |
| Number of guard subcarriers | 52 | 105 | 211 | 423 | 635 | 847 |
| Number of RB | 6 | 15 | 25 | 50 | 75 | 100 |
| Sample Rate (MHz) | 1.92 | 3.84 | 7.68 | 15.36 | 23.04 | 30.72 |
| Symbols/Subframe | 7/6 (short/long CP) | | | | | |
| Short CP Length ($\mu$ s) | 5.2 first symbol, 4.69 six following symbols | | | | | |
| Long CP Length ($\mu$ s) | 16.67 | | | | | |

Table 2.1: LTE Standard parameters

In the frequency domain, the number of subcarriers varies from $N = 128$ to $N = 2048$ despite $N = 512$ and $N = 1024$ are the most used dimensions, corresponding to a channel bandwidth of 5 and 10 MHz respectively. However, the truth is that not all subcarriers are used, as some of them are guard or for example, the DC, that is not either used (see Table 2.1 for more details regarding LTE parameters). The way subcarriers are assigned is done by means of the so called Resource Blocks (RB), consisting of 12 consecutive subcarriers (180 KHz as there is a spacing between subcarriers of 15 KHz) during the whole slot (0.5 ms). Finally, the smallest unit is the Resource Element (RE), which is defined as one subcarrier during one symbol. Thus, each RB is composed by $12 \cdot 7 = 84$ RE for normal CP length (72 for extended CP).

The last part of the section is focused on the UL-PHY layer and the training sequences. There are two types of training: the Demodulation Reference Signals (DM-RS), which are based on Zadoff-Chu (ZC) sequences and the Sounding Reference Signals (SRS), used for scheduling. We must say that during the rest of the work, we will refer to the OFDM/SC-FDMA symbols directly as symbols or frames, just to clarify that it is not the same as the radio frames described above.

### 2.2.2 Physical Layer Uplink

As the rest of the work is focused on the uplink, instead of dealing with OFDMA, SC-FDMA will be the implemented technology. In the previous sub-section, it was mentioned that for the UL, a pre-processing of the complex symbols is needed in order to reduce the PAPR, mainly. Such pre-processing is done by means of a $M$-point FFT, which can be understood as a spreading of the data symbols over the whole bandwidth associated to that device. Once the $M$-point FFT is done, the new $M$ symbols are mapped into the subcarriers of interest. There are two types of mapping, localized and distributed, and, once it is done, as for the OFDMA case, the $N$-point IFFT is applied (check Figure 2.3 to see the full block diagram to generate the SC-FDMA symbols). Despite this two-step operation, signals in both modes have simple time-domain representations. Again, supposing

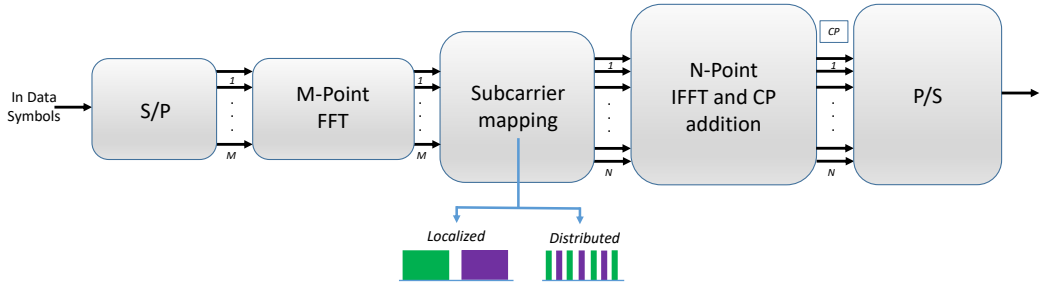


Figure 2.3: Modules needed to obtain the SC-FDMA signal

a set of M complex symbols $\mathcal{S} = \{s(1), s(2), ..., s(M)\}$, the SC-FDMA signal for both cases is given by:

### Localized SC-FDMA

$$x(n) = \begin{cases} \frac{1}{Q}\, s(p) & n = p\,Q \quad 0 \leq p \leq M-1 \\ \sum_m s(m) c_m & \text{otherwise} \end{cases}$$

### Distributed SC-FDMA

$$x(n) = \frac{1}{Q} s(n \bmod M)$$

where $Q = \frac{N}{M}$ is also known as the spreading factor, and, $c_m$ represent complex values resulting from the previous operations, but we will not enter into detail of such development.

### 2.2.3 Reference Signals

An important feature of every system are training sequences. These signals are used for synchronization, channel estimation and other features needed to establish a reliable link which are sent every 6 or 7 SC-FDMA symbols (depending on the length of the CP). In this case, they are based on Zadoff-Chu (ZC) sequences, that have interesting properties making them suitable for these systems, such as a good auto-correlation and cross-correlation. Furthermore, as they have unitary module, there is no need of applying the $M$-point FFT done at the SC-FDMA transmitters, the $N$-point IFFT is enough. Denoting the number of users/transmitters by $N_u$, each one of them has been assigned $N_i^{RS}$ orthogonal subcarriers, $i = 1, 2, ..., N_u$. For the LTE case (and this one too), $N_i^{RS} = 12\, N_i^{RB}$, where $N_i^{RB}$ stands for the number of resource blocks assigned to the $i$-th user. Defining $N_i^{ZC}$ as the largest prime number smaller than or equal to $N_i^{RS}$, ZC sequences follow the next expression:

$$zc_q(n) = e^{-(j\frac{\pi q n(n+1)}{N_i^{ZC}})} \tag{2.2}$$

for $i \in [1 : N_u]$, $n \in [1 : N_i^{ZC}]$. The sequence defined in (2.2) is cyclically extended to $N_i^{RS}$ as follows: $zc_q^{ex}(n) = zc_q(n \bmod N_i^{ZC})$. In case $N_i^{RB}$ equals 1 or 2, special training sequences are defined for LTE. As in this work, for simplicity, $N_i^{RB} \geq 3$, we will not enter into details of these special sequences. It is easy to see that there is a correspondence between $M$ and $N_i^{RS}$, both playing the roll of the number of transmitted symbols or the number of used subcarriers per user. Formally, it should be $M_i$, as not all users will use the same number of sub-carriers, but in order not to overload with notation, $M$ will be used indistinctly. Once the IFFT of this sequence is done at each UE, it is transmitted through the channel. At the receiver side, as these sequences are known, beamforming and channel estimation techniques can be applied.

## 2.3 SDMA

The Space-Division-Multiple-Access (SDMA) technique is a widely used channel access method in systems where there are multiple antennas at the transmitter and/or the receiver. It consists of creating a set of orthogonal spatial channels while in other domains, such as time and/or frequency, there can be a reuse of the resources. By means of using smart antennas, able to point at particular directions, SDMA is capable of serving multiple users within the same cell or region.

Since the beams that point the devices are focused (ideally, they are infinitely narrow), it allows having more users than if this technique were not used, covers greater ranges with less radiated energy and provides a gain in the signals that is of capital relevance when demodulating them.

Prior to the implementation of this access method, the BSs had no information on the position of the devices, therefore they radiated signal in all directions. As we can imagine, much of the power is wasted with the addition of creating interferences to other cells. However, using SDMA allows having a particular radiation pattern, adapted to each device, trying to obtain the maximum gain in the direction of the user of interest. In particular, SDMA allows creating beamformers, which in fact is the key point of this work. As mentioned in the introduction, beamformers are created thanks to a prior knowledge by the BS on how the user will transmit the training sequences. For example, in 4G-LTE, beamformers are created thanks to a time-reference signal. The BS will try to find out which is the direction from where the time-reference signal is coming from. In our proposal for 5G, the BS will look for repeated sequences inside the symbols to create the combiner.

## 2.4 NOMA

As seen in previous sections, LTE provides orthogonality in the frequency domain, as it does not allow frequency overlapping between users. Despite that, due to the structure of SC-FDMA, interference from other users will be found even if beamforming techniques are used. However, maybe the main drawback is that such technology supports a maximum number of users that can be relatively low in comparison to mMTC. Therefore, for the 5G case, one question arises: what happens when the number of devices requesting resources is greater than the available ones? In other words, how can we solve one of the key features of the 5G, that is allowing mMTC.

Apart from achieving higher data rates and low latency, with the appearance of mMTC in 5G, the roll these kind of communications will play in the next generations will be very important, being the base for IoT applications, for example. This problem of providing massive connectivity with a limited number of resources is addressed by the Non-Orthogonal Multiple Access (NOMA) solutions. As the multiple access is one of the most critical points in every technology, we prefer to state the main differences between the two main access schemes at the physical level, which are the Orthogonal (OMA) and Non-Orthogonal Multiple Access (NOMA). In OMA, each user can transmit its signal exploiting an orthogonal channel, as there is a way to distinguish users either by time, frequency or code (TDMA, FDMA, CDMA or OFDMA). In NOMA, users can use the same non-orthogonal resources yielding to a higher spectral efficiency. There are mainly two types of NOMA: Power-Domain multiplexing (P-NOMA) and Signature-Based (S-NOMA). For the Power-Domain case, users are allocated power taking into account their channel conditions in order to optimize the overall network. Then, Successive Interference Cancellation (SIC) is applied with the aim of reducing interferences and make a correct decoding. We will not enter into detail about these schemes, as they are not used during this work. Regarding S-NOMA, there has been recent work on many schemes, such as Multiuser Shared Access (MUSA) and Sparse Code Multiple Access (SCMA) among others, which are basically a spreading of the data stream over the resources in a particular manner, trying to overcome the problem of non-orthogonality. The design of these kind of spreading functions can be based in codebook structures, delay patterns, spreading sequences and other methods, but in the end, it is a way of encoding the data using pseudo-orthogonal patterns. In particular, in this work we will assume that users make use of the Repetition Division Multiple Access (RDMA).

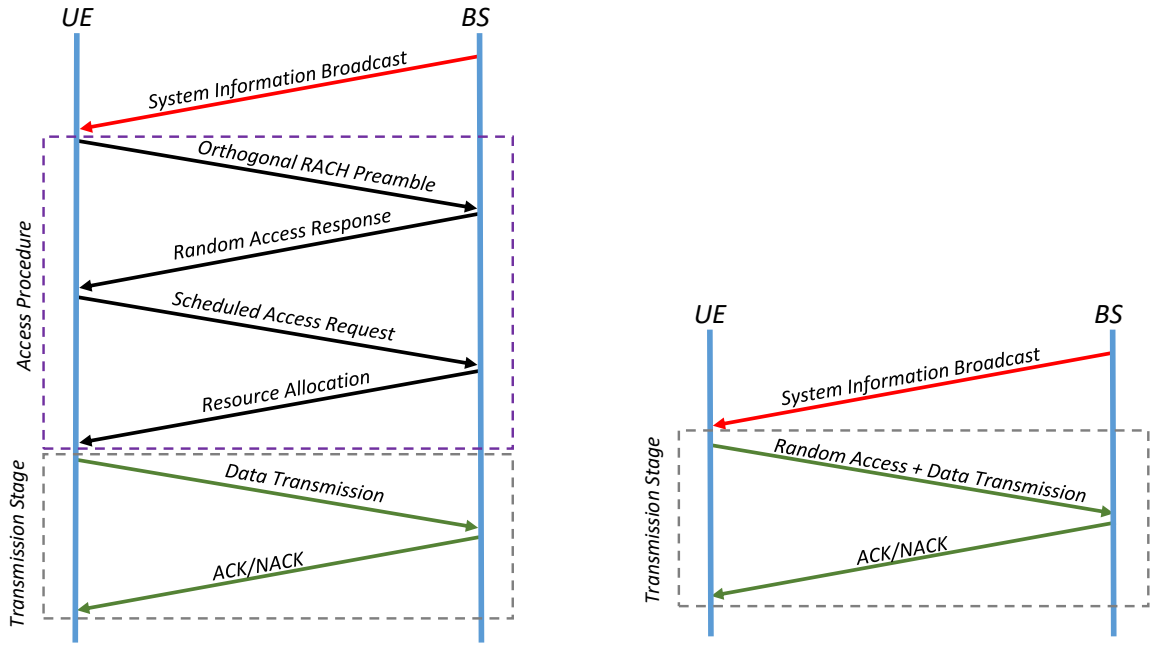


(a) Request Grant Access Procedure

(b) Grant Free Access Procedure

Figure 2.4: On the left, the RG procedure whereas on the right we show the GF method. The reader can appreciate the more steps RG has to follow in comparison to GF.

Regarding the way users access to the media, there are two main access schemes. The widely used Request Grant (RG) and the Grant Free (GF). The first one is more used, being the standard procedure in LTE. The main difference between both procedures is that RG involves mores steps than GF as it first makes the demand of resources, waits for the acknowledgment and finally starts transmitting the information, whereas GF directly sends the information. Figures 2.4a and 2.4b show better the steps that both techniques have to follow. We can see that GF accesses are faster than RG as they involve less operations.

Since both GB and GF uplink multiple access schemes do not support mMTC, our approximation is to use a novel technique to keep using them with NOMA. In particular, during the rest of the work we will suppose users directly transmit their information, being a GF scheme. In fact, autonomous GF, where the devices select the resources without restrictions and directly send the information is the one used for this part.

## 2.5 Signal Model

Last but not least, the modeling of the channel and the signal at the receiver. Let's formulate the Channel Impulse Response (CIR) in a generic way. Imagine, the length of the channel is given by $L$, the number of taps. In case $L > 1$ the transmitted signal will travel over different paths with respect to the first tap, meaning ISI and also that the channel is frequency selective (FS). We will further assume that the taps will be located at different times and positions with respect to the first one, being the tap corresponding to the shortest path from Rx to Tx and assumed to be in Line of Sight (LOS). For this work, the amplitudes and delays we have used for the CIR in a FS channel are defined by 3GPP (EPA case), being a low delay spread channel, enough for the purposes of this work, simulating pedestrian scenarios. However, there should be no problem with the proposed schemes in case other channels are tested, as we have designed our systems in order to be resilient to higher delay spread channels. EPA channel profile is summarized in the following table:

| Tap Number | Excess Tap Delay (ns) | Relative Power (dB) |
|---|---|---|
| 1 | 0 | 0.0 |
| 2 | 30 | -1.0 |
| 3 | 70 | -2.0 |
| 4 | 80 | -3.0 |
| 5 | 110 | -8.0 |
| 6 | 190 | -17.2 |
| 7 | 410 | -20.8 |

It has been mentioned that only the first tap will preserve the direction of the source, meaning that the signal traveling among other paths will arrive at the same time or delayed and from another direction with respect to the main source. In our model, such delays are fixed by the EPA model, but for the direction of arrival we allow them from deviating $[-\Omega^o\ ,\ +\Omega^o]$ with respect to the source as in WINNER models. The following scheme, with only one user, summarizes best this idea.

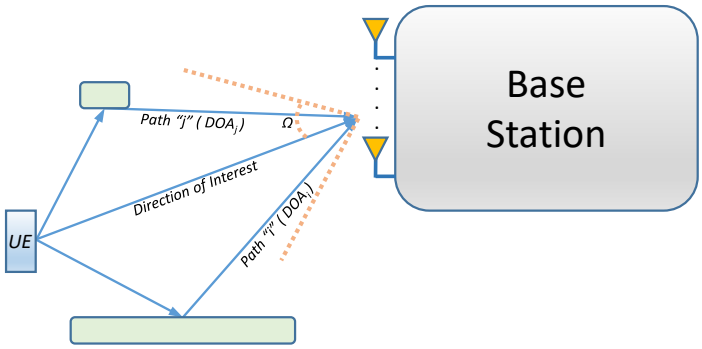


Figure 2.5: Graphical representation of a channel with multiple paths, arriving from different directions with respect to the transmitting source.

Denoting the CIR by vector $\boldsymbol{h}_i = [h_{i,0}\, h_{i,1}\, ...\, h_{i,L_i-1}] \in \mathbb{C}^{L_i\times 1}$, and $\boldsymbol{x}_i(n) = [x_i(n)\, x_i(n-1)\, ...\, x_i(n-L_i+1)] \in \mathbb{C}^{L_i\times 1}$, representing the samples of a given SC-FDMA symbol of user "$i$"(no matter if it is data or training at this point), the signal that we collect at the antennas of the BS given by $\boldsymbol{y}(n) \in \mathbb{C}^{N_a\times 1}$, where $N_a$ is the number of antennas at the receiver side, can be expressed as follows:

$$\boldsymbol{y}(n) = \sum_{i=1}^{N_u} \boldsymbol{S}_{\boldsymbol{h}_i} \boldsymbol{h}_i^* \circ \boldsymbol{x}_i(n) + \boldsymbol{n} = \sum_{i=1}^{N_u} [\boldsymbol{s}_{h_{i,0}}\, \boldsymbol{s}_{h_{i,1}}\, ...\, \boldsymbol{s}_{h_{i,L_i-1}}]\, \boldsymbol{h}_i^* \circ \boldsymbol{x}_i(n) + \boldsymbol{n} = \tag{2.3}$$

$$= \sum_{i=1}^{N_u} \left( h_{i,0}^* x(n) \boldsymbol{s}_{h_{i,0}} + h_{i,1}^* x(n-1) \boldsymbol{s}_{h_{i,1}} + ... + h_{i,L-1}^* x(n-L+1) \boldsymbol{s}_{h_{i,L-1}} \right) + \boldsymbol{n}$$

where $\circ$ represents the Hadamard product and $\boldsymbol{s}_{h_{i,l}} \in \mathbb{C}^{N_a\times 1}$ stands for the steering vector of user "$i$"coming from the angle associated to the respective tap of the channel. Compacting all steerings from a device and its respective channel we obtain matrix $\boldsymbol{S}_{\boldsymbol{h}_i} \in \mathbb{C}^{N_a\times L_i}$. In general, a steering vector whose direction of arrival is given by $\theta$, has the next formulation: $\boldsymbol{s}(\theta) = [1\ e^{-2\pi \frac{f_o}{c} D \sin(\theta)}\ e^{-2\pi \frac{f_o}{c} 2D \sin(\theta)}\ ...\ e^{-2\pi \frac{f_o}{c} D(N_a-1) \sin(\theta)}]$ where we only contemplate the elevation angle and $D$ represents the distance between antennas, which will be supposed of $\frac{\lambda}{2}$ for the rest of the work. We must say that depending on the coherence time of the channel, the angles from which arrives the multipath may vary. For example, in case the coherence time is just one SC-FDMA symbol, the direction of arrival of the multipath will change symbol by symbol. Finally,

$\boldsymbol{n} \sim N(\mathbf{0}\,,\, N_o\boldsymbol{I}) \in \mathbb{C}^{N_a \times 1}$ represents the Additive White Gaussian Noise (AWGN) found at the receiver. The reader can appreciate that this model is in fact a linear convolution between the data and the channel adding the steering vectors of each tap. The same model will be applied for the two technologies in which we work during the project.

# Chapter 3

# Blind Beamforming for 5G

During the previous chapter, the basics of NOMA were presented. It was also mentioned that one type of S-NOMA scheme was going to be implemented, being the Repetition Division Multiple Access (RDMA). Despite different S-NOMA techniques provide good performances, they do not contemplate using the signature (in this case, the position of the repeated sequence) to take benefit from the spatial subspace to create beamformers. In essence, our idea is to make use of that dimension to reduce the overall probability of collision that will happen in the frequency domain. Thus, if we are able to separate users, interferences between them would decrease and, hence, the BER would be improved.

The rest of the chapter is organized as follows: first we will see how to squeeze the actual RDMA scheme in order to create users' beamformers in a blind manner and the posterior processing the base station needs. Then, a study on the probability of collision, being the same as the probability of requesting the same resources, has been done. Finally, we provide some theoretical expressions related to the achievable rate, comparing our proposal with other state-of-the-art techniques. Each subsection contains both the developments and simulations needed to understand the steps we have followed.

## 3.1 S-RDMA

As stated in the introduction, we will try to overcome the problem of sharing the same resources by different users/devices. The idea is to add the spatial subspace to provide an extra orthogonal axis and reduce the probability of collision in a mMTC scenario. For example, let's imagine that there is a set of available frequencies and two users, located at different positions, make use of the same ones. This means that they would overlap in the frequency domain, so, apparently the receiver will have a mix of the information from both users, yielding to errors in the demodulation process. This problem can be solved by means of a beamformer being able to separate signals thanks to the spatial position of each. In other schemes the BS knew the reference signal, but in here this will not happen, being the reason of talking about blind-beamforming.

At this point, we are able to present how should be the frames in the UL in order to allow mMTC for 5G. We will call our scheme Spatial-Aimed RDMA (S-RDMA). Once the users have the SC-FDMA symbols ready to transmit, they will repeat a training sequence at two different positions inside the final symbol. We should emphasize that the BS does not need to know such pilot and can be reused by different devices (or all of them), as presented in Figure 3.1. The only requirement for the BS is to know where the training can be allocated, not their value neither their type. In this case, we will use ZC sequences, being the ones devoted for training in LTE, but as we will not estimate the channel, it is important to remark that we can use other training sequences as long as they meet that the correlation between training and data is zero, which in general is true for the training sequences used so far in previous technologies. Once we have the frames that each user will send, how do we find a spatial processor able to separate the information regarding its

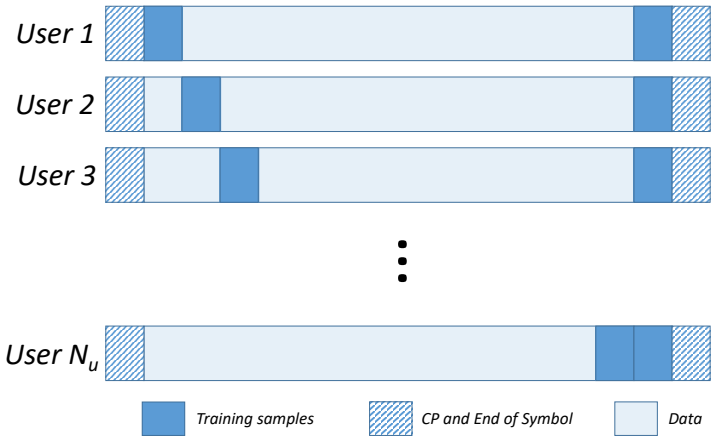


Figure 3.1: Frame structure for the S-RDMA scheme, where each user repeats in a particular time slot its training sequence. Also, to preserve the circularity of the channel, we make use of the CP.

position/direction/user in a blind manner? Thanks to the knowledge of the receiver about where the training could be located, we can formulate the following problem:

$$\begin{aligned} &\min_{\boldsymbol{b}_i} \ \mathbb{E}\{|\boldsymbol{b}_i^H \boldsymbol{x}_1 - \boldsymbol{b}_i^H \boldsymbol{x}_2|^2\} \\ &\text{s.t.} \quad 2\,\Re\left\{\mathbb{E}\{\boldsymbol{b}_i^H \boldsymbol{x}_1 \boldsymbol{x}_2^H \boldsymbol{b}_i\}\right\} = \theta \end{aligned} \tag{3.1}$$

The base station will receive the mix of all users' frames, and to create the combiner for a particular user it will need two sets of samples, the training at the first part (which is variable inside the imaginary grid) and the second part of training (fixed at the end of the frames for all users), denoted by $\boldsymbol{x}_1$ and $\boldsymbol{x}_2$. The constraint takes into account that both snapshots are correlated, which by design is true, as they share training. Defining $\boldsymbol{R}_{kl} = \mathbb{E}\{\boldsymbol{x}_k\, \boldsymbol{x}_l^H\}\, \forall\, k, l \ = \ 1, 2$, the solution to such problem is:

$$(\boldsymbol{R}_{11} \ + \ \boldsymbol{R}_{22})\boldsymbol{b}_i \ = \ (1+\lambda)(\boldsymbol{R}_{12} + \boldsymbol{R}_{12}^H)\boldsymbol{b}_i \tag{3.2}$$

$i \ = \ 1, 2, ..., N_u$, where $\lambda$ is the Lagrange multiplier. In the first set of snapshots, $\boldsymbol{x}_1$ , we will find the training of interest and data from the rest of users, while in the second part, $\boldsymbol{x}_2$, we find the contribution of all users' pilots. By means of such beamformer, the preserved signal is the one from the direction of the user that sends the same in both $\boldsymbol{x}_1$ and $\boldsymbol{x}_2$. Moreover, at the output, the rest of directions from which arrives power will be nulled. Figure 3.2 illustrates this phenomena, where we have sources at $[0^o\ 19^o\ -19^o\ -20^o\ -27^o\ 70^o]$ using $N_a \ = \ 64$ and a $SNR \ = \ 10dB$. In this case, the selected $\boldsymbol{x}_1$ only contains training from the user at $19^o$ and data from the rest, and $\boldsymbol{x}_2$ contains training from all of them. We can see that the beamformer only points to the user at $19^o$ and nulls the rest.

However, for the case where more than one user transmits its pilot in the same variable training slot $\boldsymbol{x}_1$ (see Figure 3.4), that is when inequality (3.3) is fulfilled, the combiner will point to more than one device.

$$\left\lfloor \frac{N \ - \ C_p}{T} \right\rfloor \ + \ 1 \ \leq \ N_u \tag{3.3}$$

where $N$ represents the length of the IFFT performed to obtain the SC-FDMA symbols, $T$ denotes the length of the training and $C_p$ is the number of samples of Cyclic Prefix. Figure 3.5 shows the problem of transmitting in the same training time, where we can see two sources that have transmitted training at $\boldsymbol{x}_1$, located at $[19^o\ -27^o]$ of elevation, while the other sources are placed at

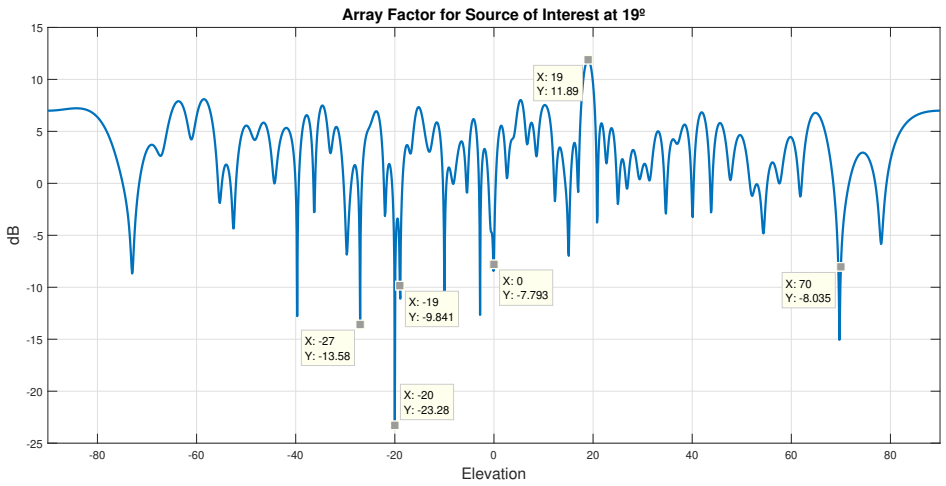


Figure 3.2: Array response for a source located at 19°. The rest of transmitting sources are nulled, as the BS is taking the snapshots $\boldsymbol{x}_1$ and $\boldsymbol{x}_2$ at the frame positions where the source at 19° is allocating its training.

$[70^o\ 0^o\ -19^o\ -20^o]$. In these cases, thanks to the great number of antennas, up to $N_a = 1024$ in some bands, sources will be clearly distinguished, allowing the receiver to estimate their positions. Once the receiver knows/estimates the Direction of Arrivals (DOAs) thanks to this first beamformer, it can apply different solutions to only point one user and demodulate its signal. In particular, in this work we propose the simplest one: $\boldsymbol{b}_{s,i} = \boldsymbol{s}_i$ where sub-index $s$ refers to "separate "and $\boldsymbol{s}_i$ is the steering from the direction the previous beamformer has estimated there is a source. Figure 3.3 is the block diagram with the steps the receiver should follow to implement this system and Figure 3.6 presents how our technique is able to point only to one source applying $\boldsymbol{b}_{s,19^o} = \boldsymbol{s}_{19^o}$ for that particular example. The simulation parameters that yield to these figures are the same as the ones used to generate 3.2.

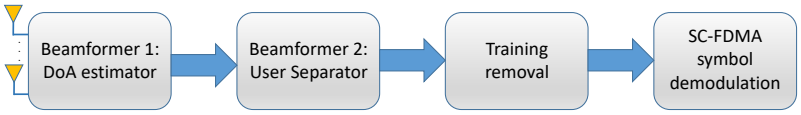


Figure 3.3: Block diagram with the steps needed to implement the S-RDMA demodulator to point user by user.

At this point, the BS, from all possible users, will only point to one of them. Another important issue that must be taken into account is the channel. Thanks to the number of antennas being used in these scenarios, we could consider that the channel will have only one tap as the BS will create such a narrow combiner that only the LOS ray will be taken into account. This realistic assumption simplifies the equalizer that must be placed at the receiver to make a correct demodulation. In particular, for the scope of this work, the equivalent channel will be just a complex number: $\boldsymbol{h}_{eq,i} = \boldsymbol{b}_{s,i}^H \boldsymbol{s}_i$. The lecturer should note that we are not compensating the amplitude of the channel, as we are supposing scenarios without great attenuation coefficients. In addition, due to the bursty nature of mMTC, devices can send the information again in case the BS does not demodulate correctly, therefore, in this case the channel is not the most critical feature.

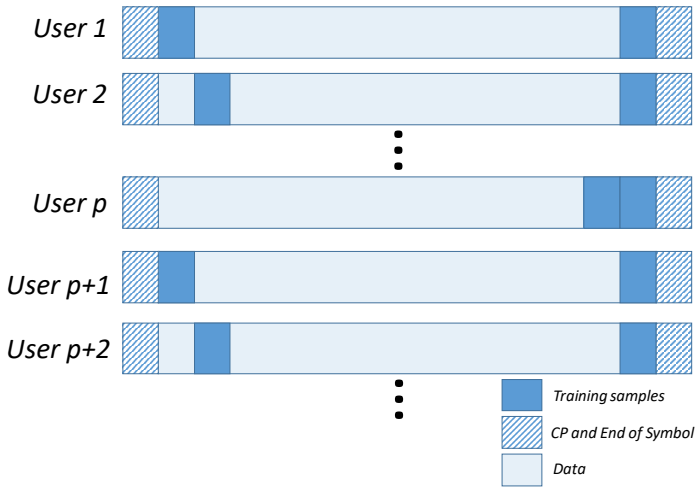


Figure 3.4: Frames for the S-RDMA scheme for the case where more than one user transmits during the same $\boldsymbol{x}_1$ period, hence, the BS will find more than one peak in the array response.

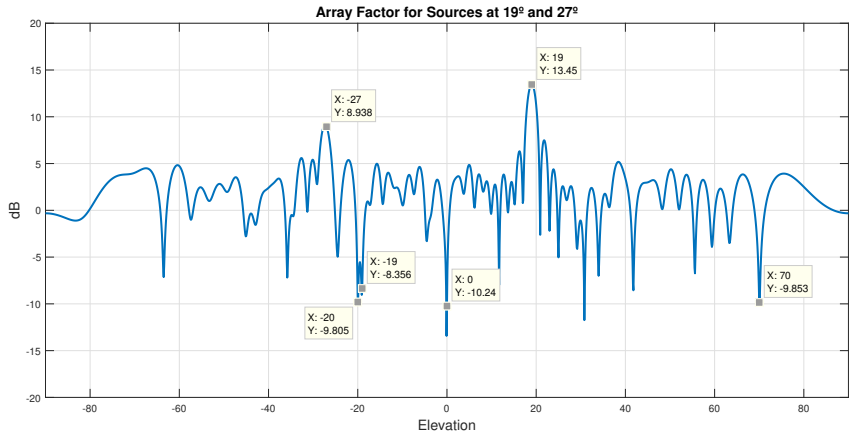


Figure 3.5: Spatial response of the blind-beamformer where two users share the same training period, located at 19º and −27º.

## 3.2 Collisions for the Proposed Techniques

Once we have seen how to distinguish users within a scenario where many devices are trying to get the resources, this section will analyze the probabilities of collision for the GF-MA to see the gain our system can provide. First, let's imagine the case where no beamforming is applied. In that scenario, plenty of users will directly pick any of the available subcarriers to transmit data. It is easy to understand, then, that a collision will occur in case two users try to get the same subcarriers. Thus, we can define the Probability of Collision in the Frequency domain, $P_{C,F}$. Before doing so, some notation should be introduced. Let's define $\mathcal{F}_i$, $i = 1, 2, ..., N_u$ as the set of subcarriers that the $i$-th user will use to transmit data, satisfying $(\bigcup_i \mathcal{F}_i) \subseteq \mathcal{F}$ where $\mathcal{F}$ refers to the complete set of available subcarriers for data. Hence, we define such probability as:

$$P_{C,F} = P\{\mathcal{F}_i \cap \mathcal{F}_j \neq \emptyset \quad \forall\,(i,j)\,,\, i \neq j\,,\, i,j = 1,2,...N_u\} \tag{3.4}$$

The reader can appreciate that it is conditioned to many parameters, such as $N_u$ and the users' bandwidth. We have seen in this chapter that the BS is able to point user by user thanks to a two-step process, therefore, in case two users send information at the same frequencies, the spatial processor will only allow the one at which it is pointing. This can be better seen in Figure 3.7a and Figure 3.7b. Figure 3.7a is the spectrum of six users that share the same bandwidth. In case no

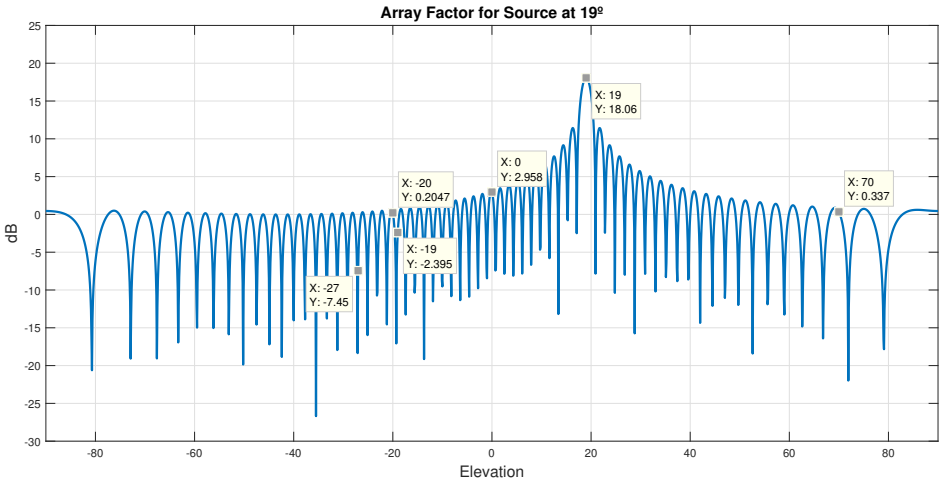


Figure 3.6: Spatial response of the second beamformer when it only points to the user at 19º using the solution: $\boldsymbol{b}_{s,19^o} = \boldsymbol{s}_{19^o}$.

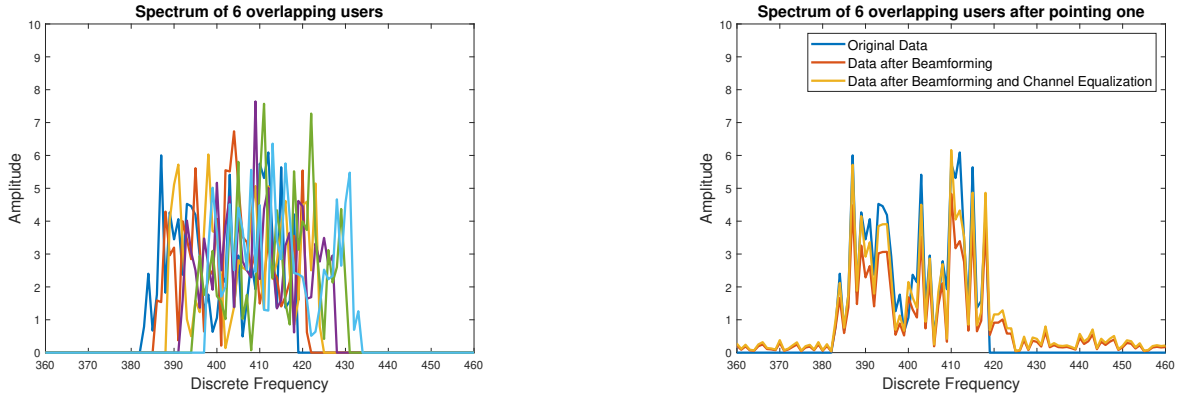


(a) Spectrum of six users overlapping users.

(b) Spectrum of the original signal (blue), filtered (red) and equalized (yellow).

Figure 3.7: On the left, six users' spectrums. On the right, after filtering, only the spectrum from the blue user is found (red) and equalized (yellow).

beamforming is applied, the receiver could not demodulate the information of any user, as it will be a mix of all the spectrums. However, Figure 3.7b presents the signal after pointing only to one user (red), compared to the original signal (blue) and after compensating the channel as we mentioned (yellow). Hence, we have adopted a way to get a probability of spatial collision, by counting the number of wrong-detected sources at the BS with the S-RDMA combiner.

For example, in the case of an onmidirectional spatial response, e.g. $N_a = 1$, there will be only one beam, covering all possible angles, therefore we could not make any kind of differentiation of users in space. On the other hand, if the beams of the estimated sources are infinitely narrow, e.g. $N_a \to \infty$, that probability will tend to zero, as the BS will detect correctly the position of the involved sources. Despite we do not propose a closed form expression, we will denote this probability by $P_{C,S}$. Finally, the overall probability of collision that will suffer our scheme, including frequency and space, is given by:

$$P_{C,SF} = P_{C,F} \cdot P_{C,S} \tag{3.5}$$

which will be upper bounded by $P_{C,F}$. Depending on the number of antennas, as they are the ones that somehow determine the width of the beams, and the length of $T$, the probability will be bigger

or lower. For this part we have generated a scenario in which at most there will be up to $N_u = 120$ devices located at different positions. The devices will request 36 or 48 subcarriers randomly. After averaging over 500 realizations for the cases where the SC-FDMA symbols are of length $N = 512$ (with an associated training length $T = 150$) and $N = 1024$ (with an associated training length $T = 300$) with different antenna size: $N_a = [16\ 32\ 64\ 128]$ if they transmit over FSs channel the results are summarized in Figures 3.8a and 3.8b.

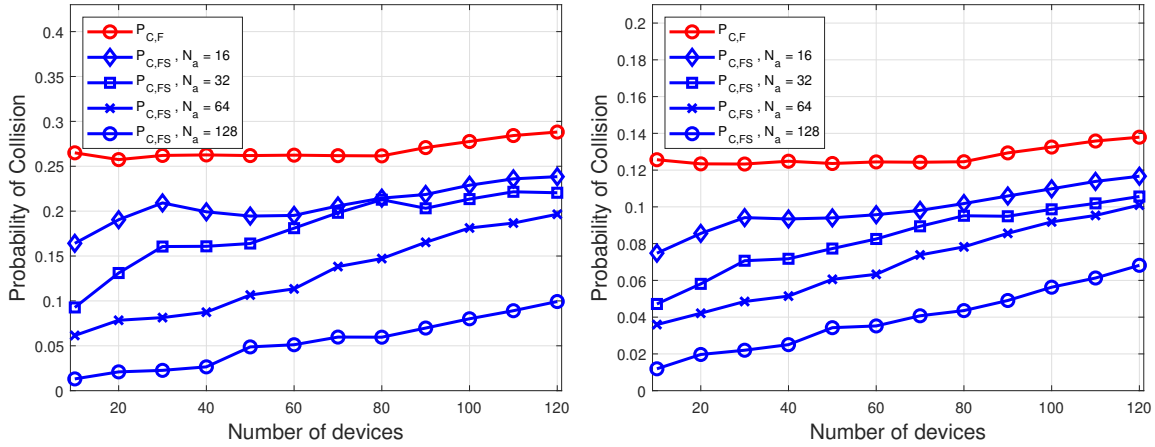


(a) Probability of collision over FS channels without (red) and with (blue) spatial diversity, for $N_a = [16\ 32\ 64\ 128]$, $N = 512$ and $T = 150$ .

(b) Probability of collision over FS channels without (red) and with (blue) spatial diversity, for $N_a = [16\ 32\ 64\ 128]$, $N = 1024$ and $T = 300$.

Figure 3.8: On the left, the variation of $P_{C,F}$ and $P_{C,FS}$ with less training than for the Figure on the right. Despite that, both show the gain our method to find sources provides to the overall system, reducing the probability of collision in the frequency domain, for different antenna array-sizes.

We can appreciate in both figures that the use of a spatial processor to discriminate users reduces the probability of collision. Despite that, the reader can note that the tendency when the number of devices increases is that all probabilities increase, which makes sense as there may be more users trying to get the same resources. However, the gain is considerable. Also, it is worthy to mention that the more antennas the receiver has, the better the performance is. This is due to the fact that if the BS has more antennas, the beams would be narrower, so, in case two sources are near, it is preferable to have more antennas to distinguish both, as it may happen that the receiver, with $N_a$ low, could consider that there is only one source an point in the middle of both. One last comment is that because users located near the endfire are more difficult to point one-on-one, we have realized that it is the main cause of such increase when using beamformers. Miss-detecting sources in high elevation angles is the main problem this system has to deal with when pointing devices, although having a large number of antennas. On the other hand, in case the majority of sources are near the broadside $P_{C,FS}$ would no longer increase at the same rates as in both figures. Finally, we can appreciate that the more training we have (Figure 3.8b, $T = 300$), the lower the probability of collision is, as we provide more accurate estimates on the involved matrices for computing the beamformers in charge of distinguishing sources.

## 3.3 Rate Analysis

Finally, the last part of the chapter presents a theoretical analysis on the Rate that a single user/device can achieve in the UL for different scenarios and technologies. For NOMA, we will assume the worst case, being the one in which all devices transmit in the same bandwidth (Figure 3.9 shows such case compared to the OFDMA case with three users), therefore apart from the multipath, interferences from other users will appear. For the case of OMA, the bandwidth associated to each

user will not suffer from interference from other users, as there is orthogonality in the frequency domain, hence, the only interference that a user can have, is the one from the multipath.

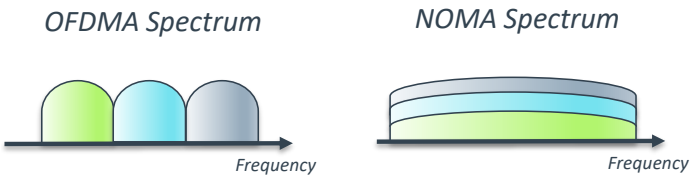


Figure 3.9: OFDMA and NOMA spectrums for three users. The OFDMA, being an OMA, preserves the orthogonality between users while NOMA does not as users share subcarriers.

At this point, we are able to formulate the achievable rate of a given user. We have developed the expressions for the case of NOMA with and without beamforming ($R_{i,N,B}$ and $R_{i,N}$), to see the gain spatial processing can give to the system, and also, for the case of OMA with beamforming ($R_{i,O,B}$) to show how NOMA could improve the rates of OMA.

$$R_{i,N,B} = (1 - P_{C,SF})\, log_2\left(1 + \frac{|\boldsymbol{b}_{s,i}^H \boldsymbol{s}_{h_{i,0}} h_{i,0}|^2}{\frac{N_o}{P}\boldsymbol{b}_{s,i}^H \boldsymbol{b}_{s,i} + \sum_{l=1}^{L_i-1} |\boldsymbol{b}_{s,i}^H \boldsymbol{s}_{h_{i,l}} h_{i,l}|^2 + \sum_{\forall j \neq i}^{N_u} \sum_{l=0}^{L_j-1} |\boldsymbol{b}_{s,i}^H \boldsymbol{s}_{h_{j,l}} h_{j,l}|^2}\right) \tag{3.6}$$

$$R_{i,N} = (1 - P_{C,SF})\, log_2\left(1 + \frac{|h_{i,0}|^2}{\frac{N_o}{P} + \sum_{l=1}^{L_i-1} |h_{i,l}|^2 + \sum_{\forall j \neq i}^{N_u} \sum_{l=0}^{L_j-1} |h_{j,l}|^2}\right) \tag{3.7}$$

$$R_{i,O,B} = \frac{1}{N_u} log_2\left(1 + \frac{|\boldsymbol{b}_{s,i}^H \boldsymbol{s}_{h_{i,0}} h_{i,0}|^2}{\frac{N_o}{PN_u}\boldsymbol{b}_{s,i}^H \boldsymbol{b}_{s,i} + \sum_{l=1}^{L_i-1} |\boldsymbol{b}_{s,i}^H \boldsymbol{s}_{h_{i,l}} h_{i,l}|^2}\right) \tag{3.8}$$

where $P$ stands for the power of the data, $P_{C,SF}$ is the probability of collision in space and frequency and the rest of parameters are the same as in previous sections . The sub-indexes in the rates denote: the user, the MA (N-NOMA, O-OMA) and B in case it uses beamforming. As mentioned, the only term that is not considered as interference is the one that arrives from the shortest path, that is a realistic assumption in outdoors or LOS environments. We have studied the case of two channels, being the first one the AWGN, which greatly simplifies the previous expressions, yielding to an achievable rates of:

$$R_{i,N,B} = (1 - P_{C,SF})\, log_2\left(1 + \frac{|\boldsymbol{b}_{s,i}^H \boldsymbol{s}_{h_{i,0}}|^2}{\frac{N_o}{P}\boldsymbol{b}_{s,i}^H \boldsymbol{b}_{s,i} + \sum_{\forall j \neq i}^{N_u} |\boldsymbol{b}_{s,i}^H \boldsymbol{s}_{h_{j,0}}|^2}\right) \tag{3.9}$$

$$R_{i,N} = (1 - P_{C,SF})\, log_2\left(1 + \frac{1}{\frac{N_o}{P} + (N_u - 1)}\right) \tag{3.10}$$

$$R_{i,O,B} = \frac{1}{N_u} log_2\left(1 + \frac{|\boldsymbol{b}_{s,i}^H \boldsymbol{s}_{h_{i,0}}|^2}{\frac{N_o}{PN_u}\boldsymbol{b}_{s,i}^H \boldsymbol{b}_{s,i}}\right) \tag{3.11}$$

We run simulations with users located at different positions between $[-90^o\ 90^o]$, each one requesting 36 subcarriers, $N = 512$ and supposing that $P_{C,SF} = 0$, meaning that such user is easy to distinguish so that the BS points him correctly with an $SNR = 15$ dB. Figures 3.10 and 3.11 show the results for both AWGN and FS channels for a user located at 19° of elevation. It is worthy to mention that the assumption of $P_{C,SF} = 0$ would no longer be valid for high elevation angles (near the limit cases of 90 and -90) because the width of the main beam varies whether it points near the broadside or the endfire. A beamformer whose beams are inside the $[-60^o\ 60^o]$ range of

elevation has a lower probability of collision in space, as the beams are narrower in that area than outside it, hence we can discriminate better sources. In addition, the computation of $P_{C,SF}$ for all the use cases we have simulated would have incurred in large computational times, therefore we have made the aforementioned assumption, that for elevation angles near $0^o$ holds. The reader can appreciate that we have included curves for different antenna sizes, being: $N_a = [16\ 32\ 64\ 128]$ with a separation between elements $D = \frac{\lambda}{2}$. Both figures have the same tendency, a decrease in the rate when the number of users increases which makes sense as there are more interferences, being one of the most critical points to deal with in NOMA. If we take a look when $N_u = 1$, there is little difference between all schemes whereas a simple increase of 10 users imply a steep decrease in NOMA rates (note that the graphic is $10log_{10}(Rate)$). However, OMA schemes provide lower rates due to the factor $\frac{1}{N_u}$, therefore it is preferable to have interferences and bigger bandwidths with a NOMA scheme. Another key point is that it is better to have small antenna-array sizes with NOMA, than greater antenna array-sizes with OMA. We can see that as all curves of NOMA with beamforming give greater rates than OMA, for both channel cases. This can be understood as it penalizes more the factor $\frac{1}{N_u}$ OMA schemes have to deal with than the interferences that will appear in NOMA.

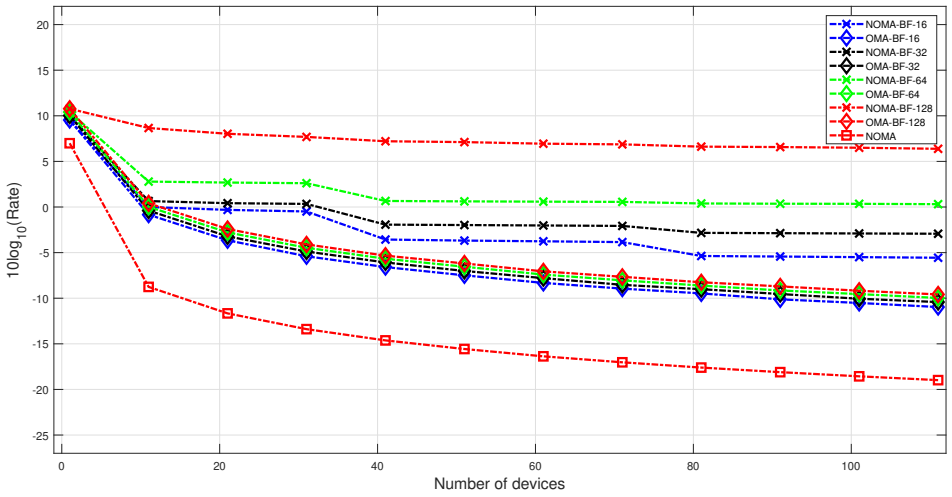


Figure 3.10: Variation of the $10log_{10}(Rate)$ of a user located at $19^o$ of elevation, for different access technologies, when the number of devices increases and for different antenna array-sizes $N_a = [16\ 32\ 64\ 128]$. The selected $SNR = 15dB$ and all users go through AWGN channels.

The second set of results shows the variation of the rate for different SNR values with the same setup that in previous simulations. Again, we have made the differentiation between the AWGN and FS channels in order not to overload with graphics in the same plot. In general, for the cases we simulated, that is $N_u = [41\ 111]$, NOMA is the best technology even in the case of having less antennas than OMA, as already stated few lines above. Apart from that, the maximum rates such user can achieve decreases when the number of users in the scenario increases, despite having good SNR conditions, meaning that interferences are the most critical issue to deal with in these cases. In addition, we can see the great gain between using spatial processing techniques for the NOMA case, where there is a large difference between both cases in all scenarios. All this information is given in Figures 3.12a, 3.12b, 3.13a and 3.13b.

From this section we can conclude that the use of NOMA techniques provide higher rates compared to OMA. We have also seen that interferences are an important issue to deal with in non-orthogonal access schemes, so there is a trade-off between sharing bandwidth and having interferences, than depending on the application must be set up. Also, there is a big gain when using a beamformer as shown in all figures, where the distance between NOMA curves with and without beamforming is large.

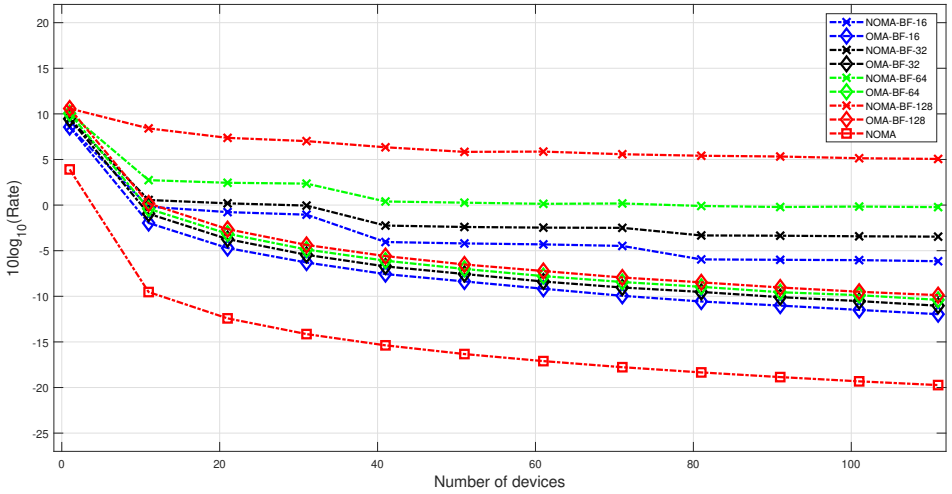


Figure 3.11: Variation of the $10log_{10}(Rate)$ of a user located at 19º of elevation, for different access technologies, when the number of devices increases and for different antenna array-sizes $N_a = [16\ 32\ 64\ 128]$. The selected $SNR = 15dB$ and all users go through FS channels.

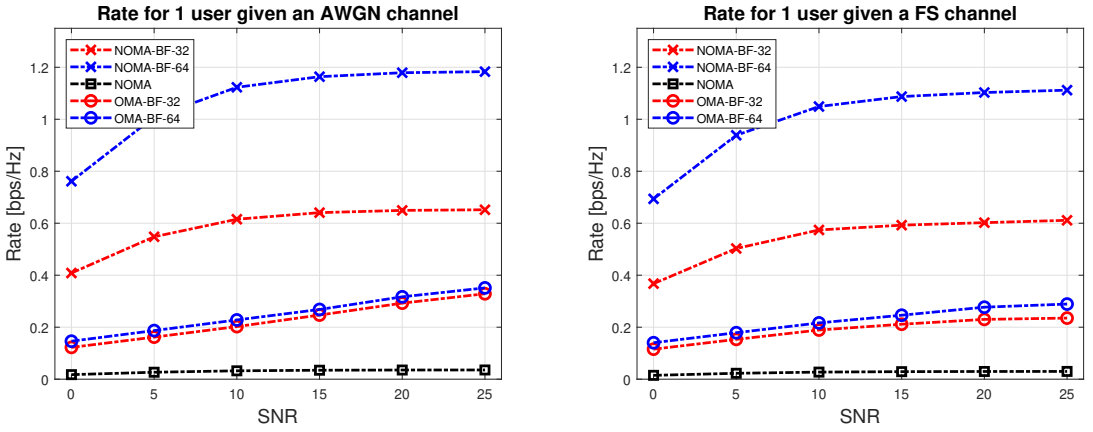


(a) Rate for a particular user, for the case of $N_u = 41$ and AWGN channels

(b) Rate for a particular user, for the case of $N_u = 41$ and FS channels

Figure 3.12: Rates for the same user for the case of AWGN and FS channels varying the SNR at the receiver when $N_u = 41$

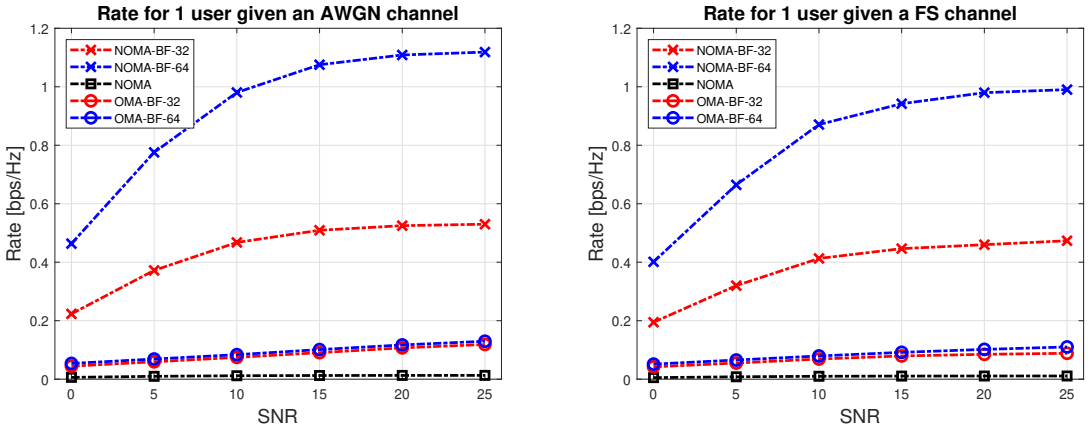


(a) Rate for a particular user, for the case of $N_u = 111$ and AWGN channels

(b) Rate for a particular user, for the case of $N_u = 111$ and FS channels

Figure 3.13: Rates for the same user for the case of AWGN and FS channels varying the SNR at the receiver when $N_u = 111$

# Chapter 4

# LTE Legacy Systems

In general, communications systems are designed such as $\frac{T_c}{T_s} >> 1$, where $T_c$ is the coherence time of the channel and $T_s$ the symbol period, to ensure the channel varies smoothly between symbols and the system is able to track that variations. It is important because failing to fulfill that condition would yield to a poor performance of the overall system, as the receiver would not be able to decode any information. For example, in LTE the coherence time of the channel is assumed to be 6 or 7 symbols, depending on the length of the cyclic prefix. In addition, it is worthy to mention that there is another important design criteria that must be met: $T_c >> T_{Training}$, where $T_{Training}$ denotes the training duration. In case it is not met, the demodulator would work with unreliable estimates of the channel, yielding to errors too. Finally, another key point that must be taken into account is the relationship between $T_{Training}$ and the reliability of the channel estimates. The more samples we devote for training, the better the estimates will be. However, if we are allocating many time to training, the efficiency of the system would decrease, therefore we can see many trade-offs between the involved parameters of the channel and the design of the systems.

Once the framework of this chapter has been established, we move forward to present our scheme. This section proposes a new frame structure to transmit the data in the UL of LTE that is able to deal with rapidly varying channels ($T_c \gtrsim T_s$) providing even higher data rates for determined lengths as we will show (despite our proposal for the UL, this idea could apply for the DL too). Along the first chapter, we presented the main features of LTE such as the training sequences, when they are sent, the frame structure and many other characteristics of this technology. Focusing on the DM-RS, they are transmitted on the third or fourth SC-FDMA symbol of an uplink slot, no matter if normal or extended CP is used. Remember that a slot, whose duration is 0.5 ms, is composed by 7 SC-FDMA symbols and that these SC-FDMA symbols are directly the output of the $N$-point IFFT and its corresponding CP. At this point we can somehow define a term that we will call Efficiency ($E$), which, actually is the same as the rate. Defining by $S_D$ the number of data SC-FDMA symbols within a slot and $S_T$ the number of DM-RS that are sent in a slot too, the following ratio gives us an idea on how many samples are we devoting to data with respect to the total:

$$E = \sum_{i=1}^{S_D} \frac{1}{S_D \ + \ S_T} \left(1 - \frac{Cp_i}{N + Cp_i}\right) \tag{4.1}$$

where $Cp_i$ refers to the number of CP samples at the $i$-th symbol (as for the Normal CP, the lengths of the cyclic prefix vary in the symbols). The intention is that the new scheme would provide higher rates with a re-allocation of the training samples along the SC-FDMA symbols different than LTE.

## 4.1 CP-TB Scheme

At this point we would like to adapt the transmission to channels whose variation is bigger than in LTE, and if possible, increase the efficiency/rate. In particular, the symbol scheme we propose is presented in Figure 4.1. We will refer to our proposal as the Cyclic Prefix Training Based (CP-TB)

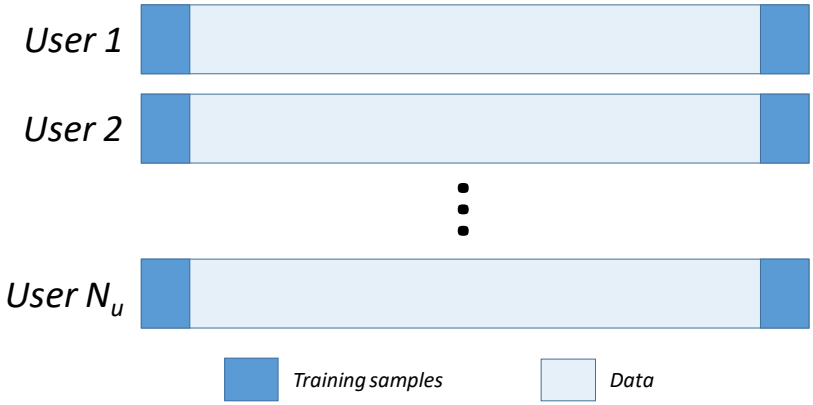


Figure 4.1: Symbol structure for the CP-TB symbols. There is a reallocation of the training with respect to LTE in the initial and final parts of each SC-FDMA symbol.

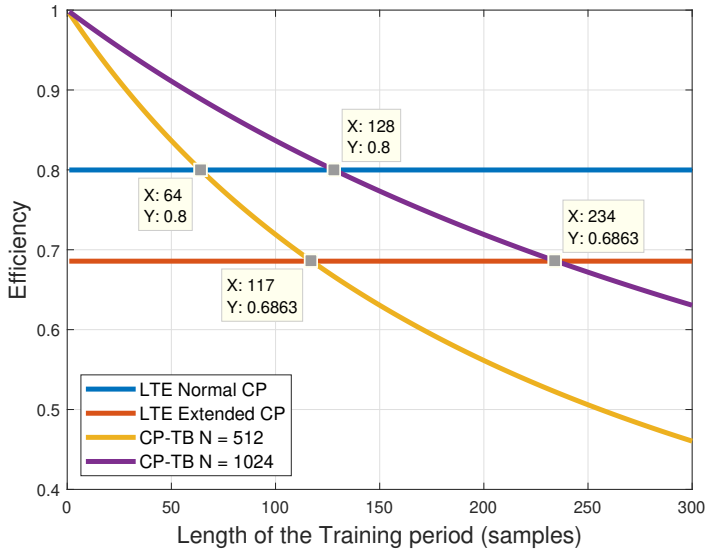


Figure 4.2: Efficiency as a function of the length, in samples, of the Training period for the CP-TB scheme and LTE standard for normal and extended CP lengths.

scheme. We can see that there are two training periods in each symbol, whose aim is to maintain the circularity of the channel. The reader should note some differences with respect to the scheme presented for 5G, but it is mainly because in this case the BS knows the training sequences of each user, so Time-Reference signal processing techniques can be used. We will refer to $T$ as the training length which are the dark blue parts of the frames. The advantages of this scheme, apart from achieving better efficiencies than LTE for different values of T, as Figure 4.2 shows, are more: easiness to track the channel and receiver synchronization among others. To have a bigger picture of the CP-TB scheme, we have included Figure 4.3, where the time-frequency grid shows the differences between CP-TB and LTE in terms of training allocation.

Before comparing the performance of both schemes, let's see which will be the involved techniques at the receiver. As it will contain many antennas, beamforming will be a mean to point users, yielding to a SDMA scheme. In particular, as the receiver knows the training sequence associated to each user, it will be a time-reference beamforming. Reminding the model presented in Chapter II, the signal at the BS antennas is given by 4.2.

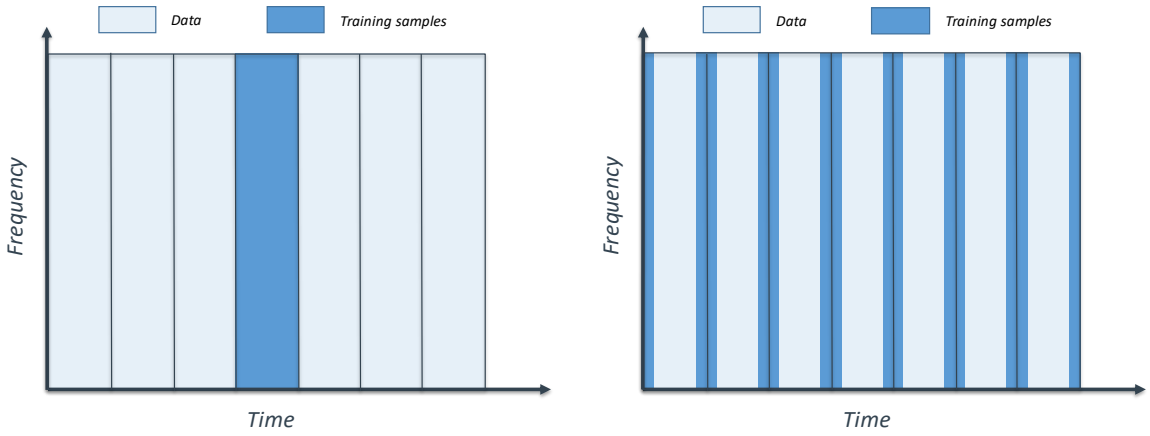


Figure 4.3: Time-Frequency grid for LTE and CP-TB systems to see better the differences between both schemes in terms of training allocation.

$$\boldsymbol{y}(n) \;=\; \sum_{i=1}^{N_u} \boldsymbol{S}_{\boldsymbol{h}_i}\, \boldsymbol{h}_i^* \circ \boldsymbol{x}_i(n) + \;\boldsymbol{n} = \sum_{i=1}^{N_u} [\boldsymbol{s}_{h_{i,0}}\; \boldsymbol{s}_{h_{i,1}}\; ...\; \boldsymbol{s}_{h_{i,L_i-1}}]\; \boldsymbol{h}_i^* \circ \boldsymbol{x}_i(n) + \;\boldsymbol{n} \tag{4.2}$$

For the case where $\boldsymbol{x}_i(n)$ is the training sequence, that is $\boldsymbol{x}_i(n) = \boldsymbol{d}_i(n)$, the beamformer will only allow the signal arriving from the user that sends the expected training sequence the receiver is waiting for. Thus, the minimization problem that gives the weights we need in each antenna is:

$$\min_{\boldsymbol{b}_i}\; \mathbb{E}\{|d_i(n) - \boldsymbol{b}_i^H \boldsymbol{y}(n)|^2\} \qquad\qquad i \;=\; 1, 2, ..., N_u \tag{4.3}$$

where, again, $d_i(n)$ represent the pilot samples, being the IFFT of the ZC sequence. This yields to the well-known Wiener solution:

$$\boldsymbol{b}_i = \boldsymbol{R}_{yy}^{-1} \boldsymbol{p}_{yd} \tag{4.4}$$

where $\boldsymbol{R}_{yy} \;=\; \mathbb{E}\{\boldsymbol{y}(n)\, \boldsymbol{y}(n)^H\}$ and $\boldsymbol{p}_{yd} \;=\; \mathbb{E}\{\boldsymbol{y}(n)\, d_i^*(n)\}$. Before giving an interpretation to the result, let's develop the correlation matrix to see which terms are there. After some algebra:

$$\boldsymbol{R}_{yy} = \sum_{i=1}^{N_u} (\sum_{l=0}^{L_i-1} \boldsymbol{s}_{h_{i,l}} \boldsymbol{s}_{h_{i,l}}^H |h_{i,l}|^2 P_d) \;+\; N_o \boldsymbol{I} \tag{4.5}$$

where $P_d \;=\; \mathbb{E}\{d_i(n)\, d_i(n)^*\}$. The reader can note that it contains power from the desired direction, the multipath and from other users. The correlation vector is: $\boldsymbol{p}_{yd} \;\approx\; \boldsymbol{s}_{h_{i,0}} h_{i,0} P_d$ thanks to the good correlation properties of ZC sequences. To easily understand the result, first let's look at the correlation matrix. In particular, its inverse can be understood as an averaging of the involved sources from where the BS is receiving power combined with noise. Next, the correlation vector exalts the direction from which the user of interest is transmitting the reference, as it contains the steering associated to that user. In the end we will only have one main beam pointing to $\boldsymbol{s}_{h_{i,0}}$ and the rest of sources will be somehow reduced/nulled thanks to the inversion of the correlation matrix.

To have a graphical result, let's see the beamformer response for the case where the user of interest is located at $0^o$ and the other users are at $[-30^o\;\; 20^o\;\; 40^o]$. Figure 4.4 shows how the combiner nulls the interfering users and only points to the one transmitting the same reference that it expects to receive. The main difference that we can appreciate with respect to 5G array responses is the width of the beams. In LTE, as the maximum number of antennas the standard supports is $N_a \;=\; 4$ we cannot achieve narrow beams. To generate that figure $N_a \;=\; 4$, $SNR \;=\; 5$ dB and the users were requesting 36 or 48 subcarriers.

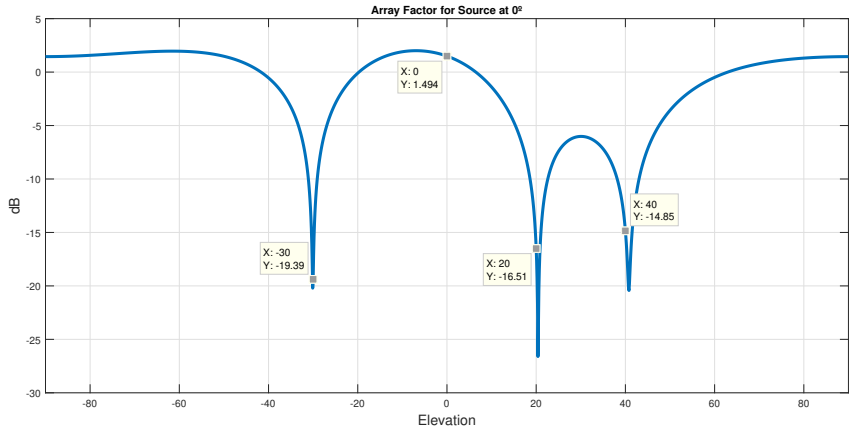


Figure 4.4: Spatial response of a beamformer whose user of interest is at 0º and the interferences are at $[-30^{\text{o}}\ 20^{\text{o}}\ 40^{\text{o}}]$, with $N_a = 4$, $SNR = 5$ dB using (4.4).

The second element that the receiver needs is the equalizer. To equalize the channel we first need to estimate it. In this work we post probably the simplest channel estimator, being the Least Squares (LS). Once the received signal passes the beamformer of interest, we will have $r_i(n) = \boldsymbol{b}_i^H \boldsymbol{y}(n) = \boldsymbol{h}_{eq,i}^H \boldsymbol{d}_i(n) + \hat{n}$, $i = 1, 2, ..., N_u$, where $\boldsymbol{h}_{eq,i}$ represents the equivalent channel, $\boldsymbol{d}_i(n)$ is the training sequence and $\hat{n}$ represents both noise and interferences at the output of the beamformer. To estimate $\boldsymbol{h}_{eq,i}$, the procedure we have followed is by means of finding the optimal value of the next minimization problem:

$$\min_{\boldsymbol{h}_{eq,i}} |\boldsymbol{r}_i - \boldsymbol{D}_i \boldsymbol{h}_{eq,i}|^2 \qquad i = 1, 2, ..., N_u \tag{4.6}$$

where $\boldsymbol{r}_i = (r_i(0), r_i(1), ..., r_i(N-1))^T \in \mathbb{C}^{N \times 1}$ and $\boldsymbol{D}_i \in \mathbb{C}^{N \times L_i}$, containing the IFFT of the ZC sequence, is defined in the following way:

$$\boldsymbol{D}_i = \begin{pmatrix} d_i(0) & 0 & 0 & ... & 0 \\ d_i(1) & d_i(0) & 0 & ... & 0 \\ d_i(2) & d_i(1) & d_i(0) & ... & 0 \\ ... & ... & ... & ... & ... \\ d_i(L_i-1) & d_i(L_i-2) & ... & ... & d_i(0) \\ d_i(L_i) & d_i(L_i-1) & ... & ... & d_i(1) \\ ... & ... & ... & ... & ... \\ d_i(N-1) & d_i(N-2) & ... & ... & d_i(N-L_i) \end{pmatrix}$$

The LS solution is given by: $\hat{\boldsymbol{h}}_{eq,i} = (\boldsymbol{D}_i^H \boldsymbol{D}_i)^{-1} \boldsymbol{D}_i^H \boldsymbol{r}_i \in \mathbb{C}^{L_i \times 1}$, that if is posted in the frequency domain, it is just the division between the observation and the training at each subcarrier. Once we have the response of the channel, the receiver just needs to equalize it by means of some of the possible techniques that are widely known. During our simulations, the frequency-domain MMSE equalizer is the chosen one, whose expression at the $j$-th subcarrier is: $Eq(f_j) = \frac{H_{eq}(f_j)^*}{|H_{eq}(f_j)|^2 + SNR^{-1}}$. Finally, after equalizing the signal, the receiver will demodulate it, providing the complex symbols. Figure 4.5 provides the complete chain to demodulate both LTE and CP-TB frames.

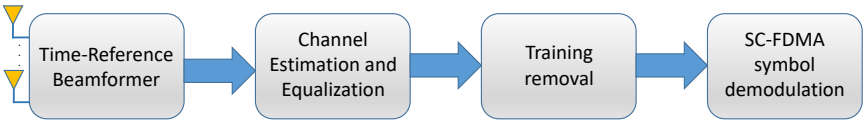


Figure 4.5: CP-TB and LTE block diagram at the receiver side.

It is easy to understand that the more samples we devote to training, the better the beamformer and channel estimator will be. Despite that, there is a trade-off between our new model and the coherence time of the channel. In case the channel remains stable during 7 or 6 symbols (short or long CP lengths) as in LTE, there will not be any advantage, as LTE uses a complete symbol to create the beamformer and estimate the channel every 7 or 6 symbols.

However, if we focus in the case of rapidly varying channels, e.g. $T_c < 6$ symbols, being the objective of this part, due to the fact that our frame structure contains training in each symbol, we are able to track the channel providing a better performance in terms of BER and also, depending on the length of the training sequence, a higher rate as shown in Figure 4.2. This result is shown in Figure 4.6, where for an SNR = 5 dB and a given user, located at $-65^o$, if we vary the coherence time of the frequency selective channel presented in previous chapters, we obtain that our system is capable of adapting to the variations of the channel, while LTE degrades its performance. In such simulations we used the parameters corresponding to a bandwidth of 5 and 10 MHz of the Long CP LTE standard (see Table 2.1) with a number of users $N_u = 10$ each one positioned at $[0^o \ -30^o \ 10^o \ 20^o \ 60^o \ -25^o \ -65^o \ -10^o \ 75^o \ -45^o]$ of elevation, requesting 36 subcarriers each for $N = 512$ and 72 subcarriers for $N = 1024$, and the values of training length, $T$, that are shown in the legend.

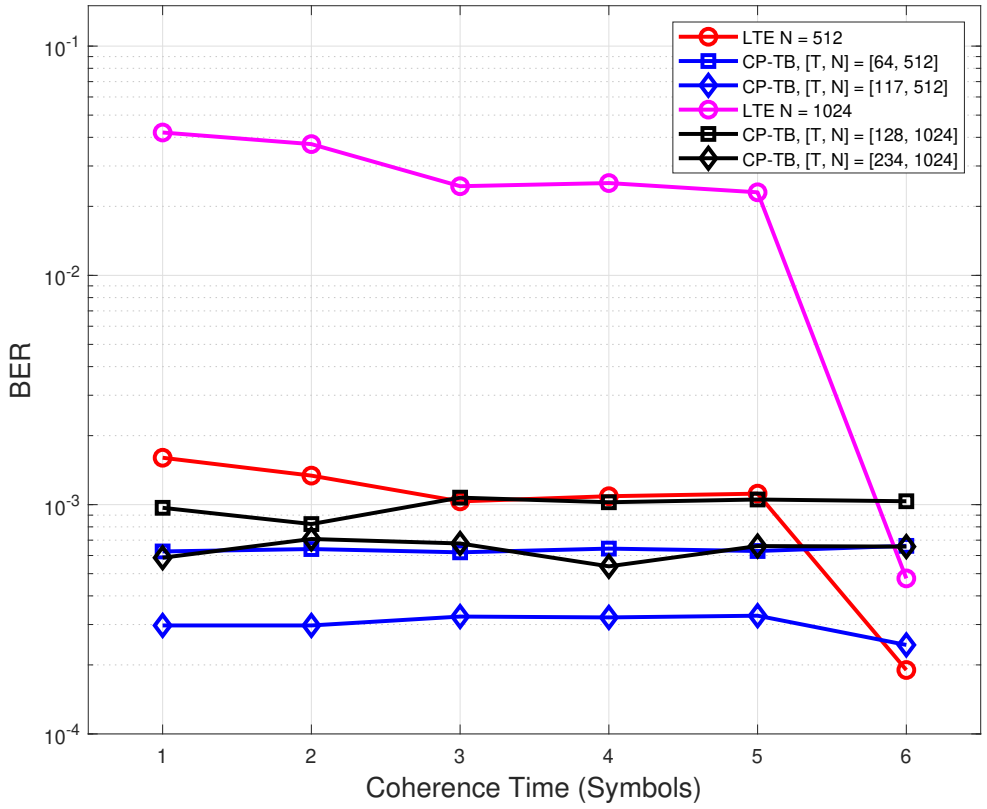


Figure 4.6: Variation of the BER for the LTE and CP-TB schemes as a function of the Coherence Time (in symbols) of the wireless channel presented in Chapter 2.

As we can see, our scheme adapts better to the variations of the channel maintaining the BER. As LTE assumes that $T_c$ is 6 (Long CP case) and sends training every 6 symbols, its performance is degraded when that coherence time is reduced, while CP-TB maintains the BER due to the training reallocation in each symbol. Moreover, focusing in the points where the coherence time is 6 symbols, we can see that for the case where $N = 512$ the distance between our scheme and LTE is higher

than for the case where $N = 1024$. This is due to the fact that when we increase the value of $N$, implicitly, to have the same rate as for LTE, a bigger number of $T$ can be used, that is we can devote more samples to train our system and hence, reduce the gap between our proposal and LTE even if the coherence time is 6 (or 7) symbols. In the limit case, we would achieve the same LTE BER when the coherence time is 6 (or 7) symbols, and maintain it for the rest of values while LTE would degrade its performance.

## 4.2 Super-Imposed

The last part of the chapter is devoted to study a further implementation of the CP-TB scheme, where, the training would be super-imposed to the data as Figure 4.7 shows. Hence, the effective rate would be one, as during the whole symbol data would be sent. In this case, we will try to find which is the optimal power allocation to data and training, when sent at the same time, to maximize the SNR at the receiver side.

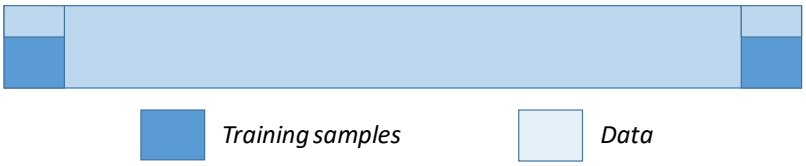


Figure 4.7: Distribution of the training and the data in this new scheme.

Let's begin with the model we will apply in this section. As stated, during some parts of the frame we will super-impose to the data, training. Apart from that, we will not work with the real channel but with an estimate of it, as the receiver will not deal with its exact value, which implies the appearance of an error with respect to the real CSI. Before taking into account such error and the training removal, the complete model the receiver has is given by:

$$y(m) = \sqrt{\alpha P}\, i(m) \otimes h(m) + \sqrt{(1-\alpha)P} d(m) \otimes h(m) + n(m) \tag{4.7}$$

where $d(m)$ denotes the training and $i(m)$ the data/information, both normalized to a unitary power value, therefore, the quantity we devote to each is controlled by $P$ and $\alpha$. Finally, $n$ refers to the AWGN noise. Once the receiver estimates the channel, denoted by $\hat{h}(m)$ with its error, given by $\tilde{h}(m)$, it will remove the training part, but still will remain some of it due to the error in the estimate. Finally, the complete model after training cancellation is:

$$y'(m) = \sqrt{\alpha P}\, i(m) \otimes (\hat{h}(m) + \tilde{h}(m)) + \sqrt{(1-\alpha)P} d(m) \otimes \tilde{h}(m) + n(m) \tag{4.8}$$

Previous to the definition of the $SNR$ to be optimized, we should define some terms that will appear in such expression. First, as we will estimate the channel, we need to quantify the power of its error. The channel estimate given by the LS technique is:

$$\hat{h}(m) = \frac{1}{\sqrt{(1-\alpha)P}2T} \int_s y(m+s) d^*(m) ds = \tag{4.9}$$

$$= \frac{1}{\sqrt{(1-\alpha)P}2T} \int_s \left( \int_r i(r+s+m)h(r)dr + \int_r d(r+s+m)h(r)dr + n(s+m) \right) d^*(m) ds$$

where, again, $T$ refers to the length of the training slot. Calculating the expected value of such estimate squared, we obtain that:

$$E_{\hat{h}} = \frac{\alpha E_h}{(1-\alpha)2T} + E_h + \frac{N_o}{(1-\alpha)P2T} \tag{4.10}$$

where the first and third term are pure interferences. Thus, defining as $SNR_o = \frac{PE_h}{N_o}$, the overall $SNR$ at the receiver will be:

$$SNR = \frac{\alpha SNR_o - \frac{\alpha}{1-\alpha}\frac{1}{2T}(\alpha SNR_o + 1)}{1 + \frac{\alpha}{1-\alpha}\frac{1}{2T}(\alpha SNR_o + 1) + \frac{1}{2T}(\alpha SNR_o + 1)} \approx \frac{\alpha SNR_o - \frac{\alpha}{1-\alpha}\frac{1}{2T}(\alpha SNR_o + 1)}{1 + \frac{\alpha}{1-\alpha}\frac{1}{2T}(\alpha SNR_o + 1)} \quad (4.11)$$

For the values of $T$ that we are supposing (more than 50 samples approximately), the third term in the denominator could be neglected, yielding to a much more easy expression to manipulate in order to find the optimal point of $\alpha$. Doing such approximation, the optimal value has a closed form expression given by:

$$\frac{\partial SNR}{\partial \alpha} = \frac{2T\big(2T(\alpha-1)^2 SNR_o - (\alpha SNR_o + 1)^2\big)}{\big(2T(\alpha-1) - \alpha(\alpha SNR_o + 1)\big)^2} = 0 \quad (4.12)$$

$$\alpha_{opt} = \frac{1 - \frac{1}{\sqrt{SNR_o 2T}}}{1 + \sqrt{\frac{SNR_o}{2T}}} \quad (4.13)$$

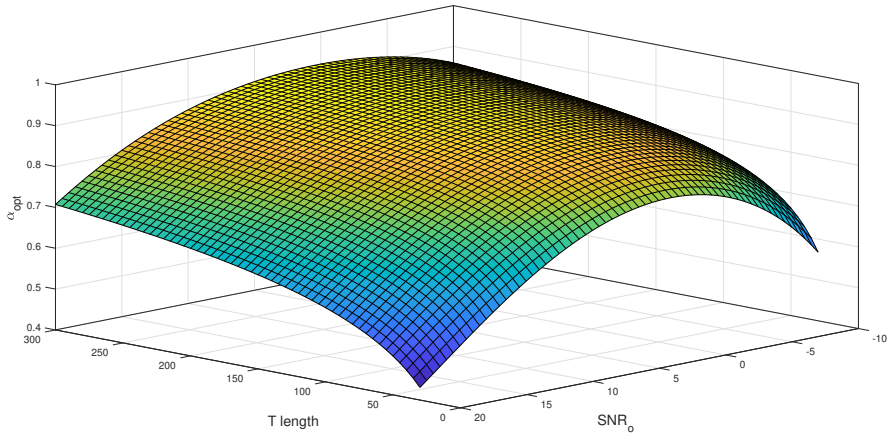


Figure 4.8: Optimal value of $\alpha$ as a function of the $SNR_o$ and $T$.

We can see an interesting point in the previous figure. In general, if the training length increases, the optimal value of $\alpha$ does too, meaning that despite we contaminate more the information (greater $T$), it is compensated by allocating more power to the data, as a higher value of $\alpha$ can be used. Such tendency is maintained for the different $SNR_o$ values. We can also appreciate that for low values of $T$ the curves of $\alpha$ with respect to the $SNR_o$ are more severe, while for high values of $T$, the variation of $\alpha$ as a function of the $SNR_o$ is less pronounced.

# Chapter 5

# Conclusions

This final chapter posts the conclusions that can be obtained once this Master Thesis came to an end. Chapter 3 presented a novel technique for allowing a massive number of devices to share the environment, and hence, the resources in a non-orthogonal manner. There, we presented the signal processing techniques needed at the BS to distinguish sources even if they transmit in the same frequencies. In the general scenario, as we will have many devices, the BS will need a second beamformer, that is capable of pointing users one by one. We also showed that the implementation of such beamformers allow to decrease the probability of collision it is likely to happen in these scenarios. Thanks to that, there are some benefits regarding BER and/or achievable Rate as we have shown, apart from decreasing the impact interferences from other users have. To summarize, that chapter shows the main benefits of taking advantage from the spatial subspace using the RDMA scheme. We can extend our contributions to other S-NOMA schemes, as we can see that blind-beamformers can be created taking into account the type of signature the system is using.

For the second technology we have focused on this work, 4G-LTE, we have proposed an interesting system that provides good performances for the case where the system has lower coherence times than the ones supposed in LTE. That could be useful as these multi-carrier solutions, and in particular OFDM, are said to be important for upcoming applications with these kind of channels. In that chapter, we showed that our system maintains the BER due to the re-allocation of the training with respect to LTE. Moreover, we almost achieve similar BERs for the cases where the coherence time of the channel is the same as in LTE, depending on the amount of training we are devoting in each symbol. Despite we can extrapolate such result to more generic scenarios, we must say that there may be set ups for which we can even outperform more LTE, or that our system and LTE are closer. It would depend on the topology, but in average, the so-called TB-CP scheme will be more suitable for rapidly varying channels. Finally, in that section we conclude with the theoretical optimal power allocation that should be done if we want to even achieve a higher rate mixing data and training at the same time.

Some future lines regarding the first technique we present could be to study if we can simplify even more the BS. One possible path could be to see if there is any kind of scheduling of the training in the frames, that allows having more users without the necessity of a second beamformer. Another point that can be investigated is the creation of beamformers with other S-NOMA schemes, such as the ones based on code or delay patterns.

Regarding the LTE Legacy system we have proposed, our guess is that it could be implemented in real systems. However, further study in particular points would be interesting with the aim of ensuring a good performance of the complete technology. For example, we are assuming that we do not have problems in terms of synchronization, which may be tested in real systems.

# Appendices

# Appendix A

# Budget

In this chapter the total cost of the project, as well as the implementation of the software, taking into account licenses, servers and wages is estimated.

The work has been done using Matlab. At least, it is needed one license in order to perform all the simulations. Apart from the software, there is another important aspect to take into account, which are the servers. Some of the simulations, due to its high computational cost, have been done in a server. The following table summarizes its main features and prize:

Table A.1: Server features

| Architecture | Operating System | Number of CPUs | Speed of CPUs | RAM | Approximated price |
|---|---|---|---|---|---|
| 64 bits | Linux | 10 | 10 | 30 | 60 € |

Finally, the last part to be taken into account for the budget are the wages. The study and implementation of the algorithms has been developed by a junior engineer during half a year. The work started February 6th and ended on June 25th, which involves 20 weeks at a rate of 35h/week. The typical wage for a junior engineer is about 17 €/h, so the total stipend for the worked hours is:

$$17\ €/\text{h} \cdot 35\text{h/week} \cdot 20\ \text{weeks} = 11900\ €$$

Apart from the junior engineer's wage, the coordinators' one must be taken into account. This work has been directed by a single director and during the 20 weeks, there has been a dedication of 6 hours per week. The typical wage for a licensed teacher at the UPC is about 42 €/h, so the total price for the worked time is:

$$42\ €/\text{h} \cdot 6\text{h/week} \cdot 20\ \text{weeks} = 5040\ €$$

By summing each one of the concepts of the work, it is obtained that the total cost of the project is about 17000 €.

# Appendix B

# Work Plan

## B.1 Work Packages, Tasks and Milestones

The different work packages are:

1. WP1: Project Planning: organization of the work at the beginning of the project. Its main objective is to plan the start and end dates for the different tasks. The start and end dates for this package were 15/02/2019 and 02/03/2019.

2. WP2: Project Goals: define the main goals and objectives of the project. The planned start date was 22/02/2019 and the end date on 02/03/2019.

3. WP3: Specifications: define the specifications the project must satisfy, such as the standards that will serve as starting point and other important parameters to establish the framework. The dates were 01/03/2019 to 12/03/2019.

4. WP4: 4G-LTE and CP-TB: learn the basics of 4G-LTE and develop the new scheme we propose with the theoretical developments and the code to simulate the performance of these two technologies. The starting date was 22/02/2019 and the end date was 26/03/2019.

5. WP5: NOMA: learn the basics of NOMA and develop the new scheme we propose with the theoretical developments and the code to simulate the performance of our scheme compared to OMA. The starting date was 27/03/2019 and the end date was 08/05/2019.

6. WP6: Simulation and Testing: simulate the performance of the two proposed technologies. Its start and end dates were: 01/05/2019 and 9/06/2019.

7. WP7: Writing up of the project: write the work and the results obtained during the project. This work package started at the very beginning, on the 01/03/2019 and ended on June, concretely at the 24/06/2019.

## B.2 Gantt Diagram

This section contains the Gantt diagram of the project.

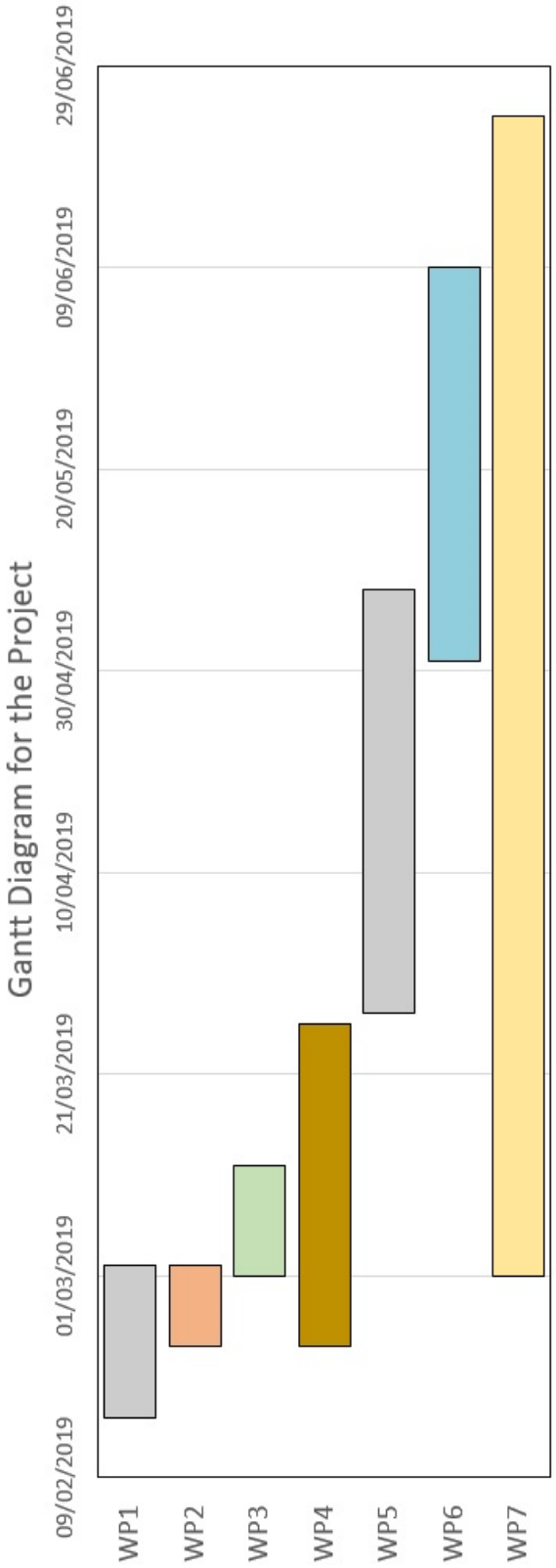


Figure B.1: Representation of the planning in a Gantt diagram.

# Bibliography


[1] Martoyo, I. and Schober, H. and Jondral, F., *CDMA versus OFDM, A Performance Comparison in Selective* IEEE Seventh International Symposium on Spread Spectrum Techniques and Applications, 2002

[2] T.Innovations, *LTE in a Nutshell* White paper, 2010

[3] Sesia, S. , Toufik, I. , Baker, M., *LTE – The UMTS Long Term Evolution* Wiley, 2011. ISBN: 9780470660256

[4] GoldSmith, A., *Wireless Communications* Cambridge university press, 2005. ISBN: 0521837162

[5] Litva, J. and Lo, TK , *Digital beamforming in wireless communications* Artech House, 1996. ISBN: 0890067120

[6] Lagunas, M.A. and Pérez Neira, A.I. and Amin, M.G. and Vidal, J., *Spatial Processing for Frequency Diversity Schemes* IEEE TRANSACTIONS ON SIGNAL PROCESSING, Volume: 48, Number: 2, 2000

[7] Songnan Xi and Michael D. Zoltowski, *SINR-Max Cooperative Beamforming for Multiuser MIMO-OFDM Systems* IEEE International Conference on Acoustics, Speech and Signal Processing, 2008

[8] J.-J. van de Beek ; O. Edfors ; M. Sandell ; S.K. Wilson ; P.O. Borjesson, *On channel estimation in OFDM systems* IEEE 45th Vehicular Technology Conference, 1995

[9] Mirza Golam Kibria, Gabriel Porto Villardi, Kentaro Ishizu, and Fumihide Kojima, *Throughput Enhancement of Multicarrier Cognitive M2M Networks: Universal-Filtered OFDM Systems* IEEE Internet of Things Journal, Volume: 3, Pages: 830-838, 2016

[10] S.S. Prasad ; C.K. Shukla ; Raad Farhood Chisab, *Performance analysis of OFDMA in LTE* Third International Conference on Computing, Communication and Networking Technologies, 2012

[11] S. Ajey ; B. Srivalli ; G.V. Rangaraj, *On performance of MIMO-OFDM based LTE systems* International Conference on Wireless Communication and Sensor Computing, 2010

[12] Gupta, Akhil and Jha, R.K., *A Survey of 5G Network: Architecture and Emerging Technologies*

[13] J.-J. van de Beek ; O. Edfors ; M. Sandell ; S.K. Wilson ; P.O. Borjesson, *On channel estimation in OFDM systems* IEEE 45th Vehicular Technology Conference, 1995

[14] Bockelmann, Carsten et. al., *Towards Massive Connectivity Support for Scalable mMTC Communications in 5G networks* IEEE Access, April 2018

[15] Bockelmann, Carsten and Pratas, Nuno and Nikopour, Hosein and Au, Kelvin and Svensson, Tommy and Stefanović, Čedomir and Popovski, Petar and Dekorsy, Armin, *Massive Machine-type Communications in 5G: Physical and MAC-layer solutions* IEEE Communications Magazine, Vol. 54, June 2016

[16] Hossain, Ekram and Al-Eryani, Yasser, *Large-Scale NOMA: Promises for Massive Machine-Type Communication* IEEE COMSOC TCCN 2018

[17] Laya, A and Alonso, Luis and Alonso-Zarate, Jesus, *Is the Random Access Channel of LTE and LTE-A Suitable for M2M Communications? A Survey of Alternatives*

[18] Yuan, Zhifeng and Yan, Chunlin and Yuan, Yifei and Li, Weimin, *Blind Multiple User Detection for Grant-Free MUSA without Reference Signal* 2017 IEEE 86th Vehicular Technology Conference

[19] Du, Yang and Dong, Binhong and Chen, Zhi and Wang, Xiaodong and Liu, Zeyuan and Gao, Pengyu and Li, Shaoqian, *Efficient Multi-User Detection for Uplink Grant-Free NOMA: Prior-Information Aided Adaptive Compressive Sensing Perspective* IEEE Journal on Selected Areas in Communications, July 2017

[20] Alam, Mehmood and Zhang, Qi, *A Survey: Non-Orthogonal Multiple Access with Compressed Sensing Multiuser Detection for mMTC* IEEE Journal on Selected Areas in Communications, July 2017

[21] Wang, Bichai and Dai, Linglong and Zhang, Yuan and Mir, Talha and Li, Jianjun, *Dynamic Compressive Sensing Based Multi-User Detection for Uplink Grant-Free NOMA* IEEE Communications Letters, Vol. 20, November 2016

[22] Azari, Amin and Popovski, Petar and Miao, Guowang and Stefanović, Čedomir, *Grant-Free Radio Access for Short-Packet Communications over 5G Networks* GLOBECOM 2017 - 2017 IEEE Global Communications Conference

[23] Y. Liu and Z. Tan and H. Hu and L. J. Cimini and G. Y. Li, *Channel Estimation for OFDM* IEEE Communications Surveys Tutorials, 2016

[24] M. Biguesh and A. B. Gershman, *Training-based MIMO channel estimation: a study of estimator tradeoffs and optimal training signals* IEEE Transactions on Signal Processing, 2006

[25] B. Karakaya and H. Arslan and H. A. Cirpan, *Channel Estimation for LTE Uplink in High Doppler Spread* 2008 IEEE Wireless Communications and Networking Conference

[26] Kwan, Raymond and Leung, Cyril, *A Survey of Scheduling and Interference Mitigation in LTE* J. Electrical and Computer Engineering, July 2010

[27] E. Yaacoub and Z. Dawy, *A Survey on Uplink Resource Allocation in OFDMA Wireless Networks* IEEE Communications Surveys Tutorials, Vol. 14, 2012

[28] Mojtaba Vaezi, Zhiguo Ding, H. Vincent Poor, *Multiple Access Techniques for 5G Wireless Networks and Beyond* Springer, 2019

[29] W. Chen and and J. Smee, *5G ultra-reliable and low-latency systems design* 2017 European Conference on Networks and Communications (EuCNC)

[30] Yuan, Zhifeng and Hu, Yuzhou and Li, Weimin and Dai, Jianqiang, *Blind Multi-user Detection for Autonomous Grant-free High-Overloading MA without Reference Signal*

[31] Mohammadkarimi, Mostafa and Ahmad Raza, Muhammad and Dobre, Octavia, *Signature-based Non-orthogonal Multiple Access (S-NOMA) for Massive Machine-Type Communications in 5G*

[32] Afif Osseiran, Jose F. Monserrat, Patrick Marsch, *5G Mobile and Wireless Communications Technology* Cambridge University Press, 2016

[33] Nam, Wooseok and Bai, Dongwoon and Lee, Jungwon and Kang, Inyup, *Advanced Interference Management for 5G Cellular Networks* Communications Magazine, IEEE, May 2014

[34] D. W. Matolak, *Channel Modeling for Vehicle-To-Vehicle Communications* IEEE Communications Magazine, Vol. 48, 2008

[35] B. Vucetic and J. Du, *Channel modeling and simulation in satellite mobile communication systems* IEEE Journal on Selected Areas in Communications, 1992

[36] J. Hoydis and S. ten Brink and M. Debbah, *Massive MIMO in the UL/DL of Cellular Networks: How Many Antennas Do We Need?* IEEE Journal on Selected Areas in Communications, 2013